J. Fluid Mech. (2015), *vol.* 785, *pp.* 219–247.
doi:10.1017/jfm.2015.631

Internal structure of vortex rings and helical vortices

Francisco J. Blanco-Rodríguez[1], Stéphane Le Dizès[1,†], Can Selçuk[2,3], Ivan Delbende[2,3] and Maurice Rossi[4,5]

[1]Aix Marseille Université, CNRS, Centrale Marseille, IRPHE, UMR 7342, 13384 Marseille, France

[2]LIMSI, CNRS, Université Paris-Saclay, 91405 Orsay CEDEX, France

[3]Sorbonne Universités, UPMC Univ Paris 06, UFR d'Ingénierie, 75252 Paris CEDEX 05, France

[4]Sorbonne Universités, UPMC Univ Paris 06, UMR 7190, Institut Jean Le Rond d'Alembert, 75005, Paris, France

[5]CNRS, UMR 7190, Institut Jean Le Rond d'Alembert, 75005, Paris, France

(Received 10 April 2015; revised 10 August 2015; accepted 22 October 2015; first published online 16 November 2015)

The internal structure of vortex rings and helical vortices is studied using asymptotic analysis and numerical simulations in cases where the core size of the vortex is small compared to its radius of curvature, or to the distance to other vortices. Several configurations are considered: a single vortex ring, an array of equally-spaced rings, a single helix and a regular array of helices. For such cases, the internal structure is assumed to be at leading order an axisymmetric concentrated vortex with an internal jet. A dipolar correction arises at first order and is shown to be the same for all cases, depending only on the local vortex curvature. A quadrupolar correction arises at second order. It is composed of two contributions, one associated with local curvature and another one arising from a non-local external 2-D strain field. This strain field itself is obtained by performing an asymptotic matching of the local internal solution with the external solution obtained from the Biot–Savart law. Only the amplitude of this strain field varies from one case to another. These asymptotic results are thereafter confronted with flow solutions obtained by direct numerical simulation (DNS) of the Navier–Stokes equations. Two different codes are used: for vortex rings, the simulations are performed in the axisymmetric framework; for helices, simulations are run using a dedicated code with built-in helical symmetry. Quantitative agreement is obtained. How these results can be used to theoretically predict the occurrence of both the elliptic instability and the curvature instability is finally addressed.

Key words: vortex flows, vortex interactions

1. Introduction

Most vortices observed in nature are curved and interact with nearby vortices. Although they can often be considered locally as axisymmetric (with possibly a jet component), their internal structure is actually azimuthally deformed by local

† Email address for correspondence: ledizes@irphe.univ-mrs.fr

effects (curvature, torsion) and non-local effects (remote vorticity). These azimuthal corrections are known to be the source of short-wavelength instabilities. The description of these corrections is therefore an important necessary step for the understanding and modelling of these instabilities. In this work, the first dipolar and quadrupolar corrections to a prescribed monopolar structure are computed for a single vortex ring, an array of rings, a helical vortex and an array of helices using two methods: an asymptotic analysis in the limit of small core size and dedicated numerical simulations.

Vortex rings are simple invariant vortical states that have been studied for more than a hundred years. In an inviscid framework, vortex rings are expected to propagate at a constant speed without changing their form. Many works have aimed at determining the ring propagation speed when the ring core size is small compared to its radius (see Saffman 1992). In this limit, the most recent work is by Fukumoto & Moffatt (2000) who also includes viscous effects and computes the internal structure of a vortex ring up to third order. This analysis clearly shows that dipolar corrections are generated at first order, while quadrupolar corrections only appear at second order. The link between dipolar corrections and local curvature has been known for a long time (Ting & Tung 1965; Widnall, Bliss & Zalay 1971; Moore & Saffman 1972). In a general setting, Callegari & Ting (1978) showed how dipolar corrections depend on the local vortex curvature. These results were extended by Fukumoto & Miyazaki (1991) to account for an axial jet component within the vortex. In the present study, these asymptotic predictions are retrieved and compared for the first time to numerical simulations of finite core size vortices.

Helical vortices are more complicated than rings; in addition to their translation motion they also rotate. Many works are devoted to the rotation and translation speeds of such invariant structures (Moore & Saffman 1972; Widnall 1972; Ricca 1994; Kuibin & Okulov 1998; Boersma & Wood 1999). In particular Kuibin & Okulov (1998) and Boersma & Wood (1999) used the expression of the velocity field in terms of Kapteyn series derived by Hardin (1982) for helical filaments. These results were further extended for multiple helices by Okulov (2004) and to higher-order corrections by Fukumoto & Okulov (2005). The effect of torsion is not present in the rings. It was first characterized by Ricca (1994) for helices. Torsion also generates a dipolar correction, as does curvature, but this effect is weaker since it is of second order (see Fukumoto & Okulov 2005). Quadrupolar corrections responsible for the elliptic deformation of the inner core are also expected at second order (see for instance Fukumoto & Moffatt 2000). Such corrections are known to be generated when a vortex is subjected to an external strain field (Moffatt, Kida & Ohkitani 1994), or is exposed to the influence of other vortices (see Le Dizès & Verga 2002) or to distant parts of the same vortex, as for a ring. This quadrupolar correction has been fully computed for a single vortex ring (without jet) by Fukumoto & Moffatt (2000). In the present work, this correction is also provided for an array of rings, a single helix and an array of helices. The effect of axial jet within the vortex core is also analysed.

These asymptotic results are then compared with numerical results obtained by DNS. For rings, the spectral DNS code developed by Bolnot (2012) is used, in which axisymmetry is enforced as well as axial periodicity, allowing short-wavelength instabilities (Widnall, Bliss & Tsai 1974; Hattori & Fukumoto 2003) and the pairing instability (Levy & Forsdyke 1927; Bolnot, Le Dizès & Leweke 2014) to be filtered out. For helical vortices, the DNS code developed by Delbende, Rossi & Daube (2012*a*) and restricted to the simulation of helically symmetrical flows is used.

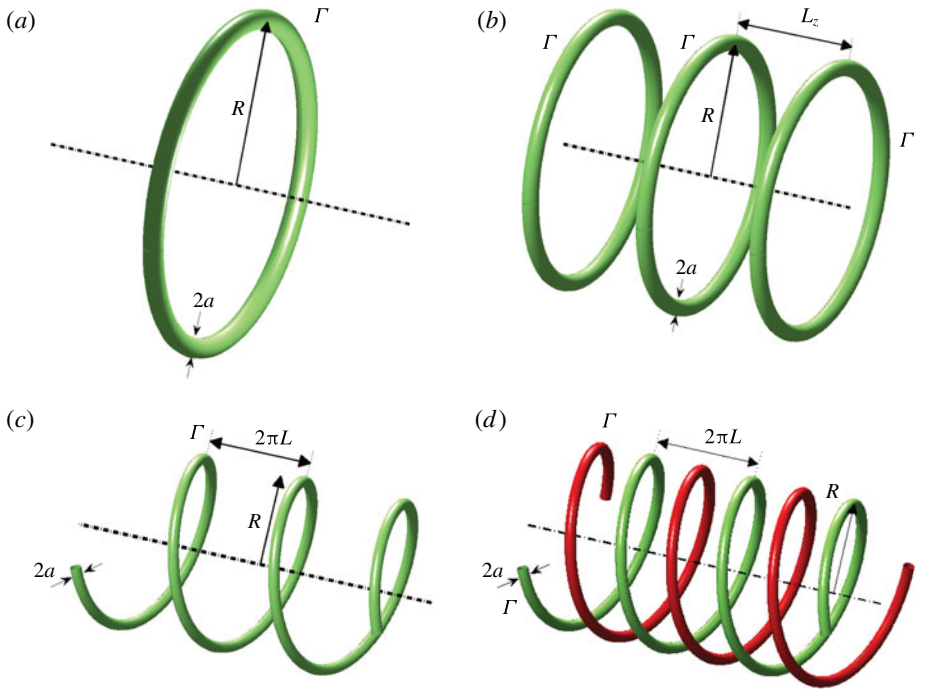

FIGURE 1. (Colour online) Vortex configurations studied in the present paper: (*a*) vortex ring, (*b*) array of rings, (*c*) helical vortex, (*d*) N helical vortices (here plotted for $N = 2$).

The paper is organized as follows. In § 2, the framework of the analysis is presented. The configurations under study are introduced, as well as the different parameters and the local reference frame in which the internal structure of the vortex is analysed. The asymptotic analysis of the inner structure is performed in § 3. Both the leading-order dipolar correction and quadrupolar corrections are obtained. The quadrupolar contribution is shown to depend on a single constant, which varies from one configuration to another. This constant is related to the external strain field experienced locally by the vortex and is computed in § 4 for each configuration. In § 5, asymptotic results are compared to DNS results. Section 6 provides a summary of the main results and a discussion of their implications concerning short-wavelength instabilities.

2. Presentation of the framework

Four vortex configurations are considered, where the vorticity field (longitudinal and transverse) is confined in a region of radius a around the curve $\mathscr{S}$, as illustrated in figure 1. Depending on the configuration, the curve $\mathscr{S}$ is

(i) a circle of radius R (figure 1*a*);
(ii) an infinite array of circles of radius R separated by a distance L_z (figure 1*b*);
(iii) an helix of radius R and pitch L (figure 1*c*);
(iv) a regular array of N helices of radius R and pitch L (figure 1*d*).

Such a curve $\mathscr{S}$ possesses a symmetry axis called the Oz axis and is parametrized by the arc length s. This means that in a global Cartesian frame, the point $C(s)$ is

given by $C(s) = (R\cos\phi, R\sin\phi, L\phi)$ with $\phi = s/\sqrt{R^2+L^2}$ (for rings, L is taken to be zero). In this Cartesian frame, the Serret–Frenet frame can be expressed as

$$\boldsymbol{t} \equiv \frac{\dfrac{\mathrm{d}C}{\mathrm{d}s}}{\left|\dfrac{\mathrm{d}C}{\mathrm{d}s}\right|} = \frac{R(-\boldsymbol{e}_x\sin\phi + \boldsymbol{e}_y\cos\phi) + L\boldsymbol{e}_z}{\sqrt{R^2+L^2}}, \tag{2.1a}$$

$$\boldsymbol{n} \equiv \frac{\mathrm{d}\boldsymbol{t}}{\mathrm{d}s} = -(\boldsymbol{e}_x\cos\phi + \boldsymbol{e}_y\sin\phi), \tag{2.1b}$$

$$\boldsymbol{b} \equiv \boldsymbol{t}\times\boldsymbol{n} = \frac{R\boldsymbol{e}_z + L(\boldsymbol{e}_x\sin\phi - \boldsymbol{e}_y\cos\phi)}{\sqrt{R^2+L^2}}. \tag{2.1c}$$

Note that the curvature κ and torsion τ of this curve are given by

$$\kappa = \frac{R}{R^2+L^2}, \quad \tau = \frac{L}{R^2+L^2}. \tag{2.2a,b}$$

The vorticity field is assumed to be uniform along the curve $\mathscr{S}$, with a constant longitudinal circulation Γ. The vorticity field is also assumed to possess a transverse component associated with a localized jet along $\mathscr{S}$. This will be further defined below. The radius a is assumed to be small compared to the other length scales i.e. R and L_z for rings, and R and L/N for helices. In this context, we are studying the internal structure within the region of radius a around $\mathscr{S}$. It is therefore useful to define a local frame centred on a point $C(s)$ of $\mathscr{S}$. Following Callegari & Ting (1978), we introduce the local polar frame

$$\boldsymbol{e}_r = \boldsymbol{n}\cos\varphi + \boldsymbol{b}\sin\varphi, \tag{2.3a}$$

$$\boldsymbol{e}_\varphi = -\boldsymbol{n}\sin\varphi + \boldsymbol{b}\cos\varphi, \tag{2.3b}$$

$$\boldsymbol{e}_s = \boldsymbol{t}, \tag{2.3c}$$

associated with the local coordinate system $(r,\ \varphi,\ s)$. The coordinate system is illustrated in figure 2 for ring and helix configurations. This non-orthogonal coordinate system is related to an orthogonal coordinate system $(r,\ \theta,\ s)$ where

$$\theta = \varphi + \theta_0(s), \quad \text{with } \frac{\partial\theta_0}{\partial s} = \tau, \tag{2.4}$$

which can be used to derive the governing equations in the local frame (see Callegari & Ting 1978, for details). In the following, the velocity vector field will be written $\boldsymbol{V} = v_\rho\boldsymbol{e}_\rho + v_\phi\boldsymbol{e}_\phi + v_z\boldsymbol{e}_z$ in the global cylindrical frame and $\boldsymbol{V} = u\boldsymbol{e}_r + v\boldsymbol{e}_\varphi + w\boldsymbol{e}_s$ in the local polar frame. The formulae that connect one representation to the other are provided in appendix A.

In the local frame, the vortex structure is assumed, at leading order, to be a columnar axisymmetrical vortex, independent of s and φ. Our goal is to determine the corrections to this axisymmetrical structure induced by the curvature and torsion of vortex lines, and the presence of distant vortices or vortical parts of the same vortex.

We introduce the following parameters

$$\varepsilon = \frac{Ra}{R^2+L^2} = \kappa a, \quad \alpha = \frac{L}{R} = \frac{\tau}{\kappa}, \quad \lambda = \frac{L_z}{R}. \tag{2.5a–c}$$

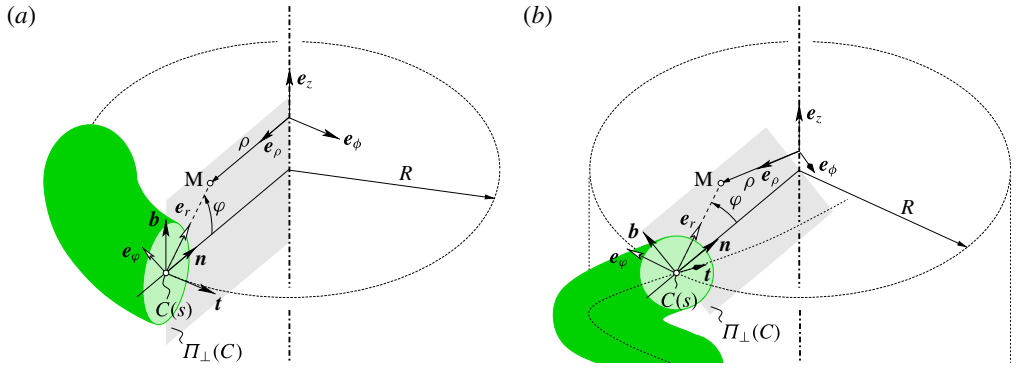

FIGURE 2. (Colour online) Illustration of the coordinate system for a ring (a) and a helix (b). The point M can be localized using the global cylindrical frame $(\boldsymbol{e}_\rho, \boldsymbol{e}_\phi, \boldsymbol{e}_z)$, or the local frames: the Serret–Frenet frame $(\boldsymbol{n}, \boldsymbol{b}, \boldsymbol{t})$ and the frame $(\boldsymbol{e}_r, \boldsymbol{e}_\varphi, \boldsymbol{t})$. Note that vectors $\boldsymbol{e}_r$ and $\boldsymbol{e}_\varphi$ are in the plane $(\boldsymbol{n}, \boldsymbol{b})$. Point $C(s)$ is defined as the point on the curve $\mathscr{S}$ which is the closest to point M.

The asymptotic analysis is performed in the limit $a \ll R$ and $a \ll L_z$ for rings, and $a \ll R$ and $a \ll L$ for helical vortices. The parameter ε is thus assumed to be small, whereas the parameters α and λ are $O(1)$. In the present study, we do not consider compressible and buoyancy effects and assume that the density is uniform and constant. Viscous effects are also neglected by assuming that the Reynolds number Γ/ν (ν is the kinematic viscosity) is sufficiently large. This hypothesis means that we consider vortex structures on time scales which are short compared to the viscous diffusion time scale a^2/ν. This allows us to consider vortical structures that translate and rotate steadily without changing their shapes. Here, we shall assume that there exists a frame translating at the velocity $V_{frame}\boldsymbol{e}_z$ where the solution is steady.

The computation of the displacement speed of helical vortices or rings has been the subject of numerous works (see for instance Saffman (1992) for rings and Alekseenko, Kuibin & Okulov (2007) for helices). In each case, there is a dominant local velocity contribution which is proportional to $-\varepsilon \log(\varepsilon)$ and oriented along the binormal vector $\boldsymbol{b}$, as predicted by the local induction approximation (Saffman 1992). This local contribution is corrected by $O(\varepsilon)$ non-local effects associated with distant vortex parts or other vortices. In all cases, the vortex structure displacement speed remains asymptotically small. The frame velocity V_{frame} is related to the vortex structure displacement speed in the manner illustrated in figure 3. For rings, the binormal vector is aligned along with the vertical axis, so the frame velocity correspond to the displacement speed $\boldsymbol{V}_{ring} = V_{ring}\boldsymbol{b} = V_{frame}\boldsymbol{e}_z$. For helices, the displacement speed can be decomposed as $\boldsymbol{V}_{helix} = V_{helix}\boldsymbol{b} = V_{frame}\boldsymbol{e}_z + W_{0_0}\boldsymbol{t}$, where $V_{frame} = \sqrt{1+\alpha^2}V_{helix}$ and $W_{0_0} = -\alpha V_{helix}$ because $\boldsymbol{e}_z \cdot \boldsymbol{b} = 1/\sqrt{1+\alpha^2}$ and $\boldsymbol{e}_z \cdot \boldsymbol{t} = \alpha/\sqrt{1+\alpha^2}$. The component W_{0_0} represents a uniform jet contribution along the vortex axis. It is only present in helices. Though small, we shall take this effect into account in our analysis.

In the uniformly translating frame, the solution satisfies the steady Euler equations. If, in the local frame, the velocity field (u, v, w) and pressure p are assumed to be independent of s, the steady Euler equations become (Callegari & Ting 1978)

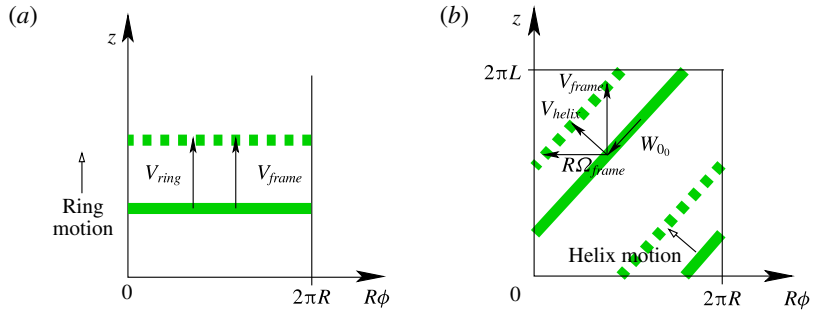

FIGURE 3. (Colour online) Definition of V_{frame} for a ring (a) and of a helix (b). The velocities $V_{frame}\boldsymbol{e}_z$ and $R\Omega_{frame}\boldsymbol{e}_\phi$ are such that their projection on the binormal vector $\boldsymbol{b}$ is equal to vortex structure displacement speed.

$$\frac{\varepsilon(-\alpha u_\varphi + w\cos\varphi)w}{h} + uu_r + \frac{v(u_\varphi - v)}{r} + p_r = 0, \tag{2.6a}$$

$$\frac{\varepsilon(-\alpha v_\varphi - w\sin\varphi)w}{h} + uv_r + \frac{v(v_\varphi + u)}{r} + \frac{p_\varphi}{r} = 0, \tag{2.6b}$$

$$\frac{\varepsilon[(-\alpha w_\varphi - (u\cos\varphi - v\sin\varphi))w - \alpha p_\varphi]}{h} + uw_r + \frac{vw_\varphi}{r} = 0, \tag{2.6c}$$

$$\frac{\varepsilon[-\alpha w_\varphi - (u\cos\varphi - v\sin\varphi)]}{h} + \left[u_r + \frac{u}{r} + \frac{v_\varphi}{r}\right] = 0, \tag{2.6d}$$

with $h = 1 - \varepsilon r\cos\varphi$. Note that, in the text, v_ρ, v_ϕ and v_z indicate the components in the global cylindrical frame, whereas the subscript indices for other variables such as the local components u, v, w refer to derivatives (e.g. $u_\varphi = \partial u/\partial\varphi$).

3. Internal vortex structure

In this section, we calculate the main dipolar and quadrupolar corrections to the local columnar axisymmetrical vortex. The velocity and pressure fields are expanded in powers of ε

$$u = +\varepsilon u^{(1)}(r,\varphi) + \varepsilon^2 u^{(2)}(r,\varphi) + \cdots, \tag{3.1a}$$

$$v = v^{(0)}(r) + \varepsilon v^{(1)}(r,\varphi) + \varepsilon^2 v^{(2)}(r,\varphi) + \cdots, \tag{3.1b}$$

$$w = w^{(0)}(r) + \varepsilon w^{(1)}(r,\varphi) + \varepsilon^2 w^{(2)}(r,\varphi) + \cdots, \tag{3.1c}$$

$$p = p^{(0)}(r) + \varepsilon p^{(1)}(r,\varphi) + \varepsilon^2 p^{(2)}(r,\varphi) + \cdots. \tag{3.1d}$$

3.1. *Monopolar structure*

At leading order, the solution is a straight vortex of azimuthal velocity $v^{(0)}(r)$ and axial velocity $w^{(0)}(r)$. The pressure $p^{(0)}$ is related to $v^{(0)}$ by

$$p^{(0)}(r) = \int_0^r \frac{[v^{(0)}(\eta)]^2}{\eta}\,\mathrm{d}\eta. \tag{3.2}$$

The longitudinal (axial) and transverse (azimuthal) distributions of vorticity are defined respectively from $v^{(0)}$ and $w^{(0)}$ by the following expressions

$$\zeta^{(0)} = \frac{1}{r}\frac{\partial}{\partial r}(rv^{(0)}), \tag{3.3a}$$

$$\Upsilon^{(0)} = -\frac{\partial w^{(0)}}{\partial r}. \tag{3.3b}$$

The asymptotic analysis can be performed for any axisymmetrical vortex with jet but for computations and numerical comparisons we use the Batchelor family of profiles

$$v^{(0)}(r) = \frac{1}{r}(1 - \mathrm{e}^{-r^2}), \tag{3.4a}$$

$$w^{(0)}(r) = W_0\mathrm{e}^{-r^2} + W_{0_0}. \tag{3.4b}$$

This vortex model is often used because it corresponds to profiles of fully viscous self-similar solutions; viscosity is then expected to modify the core size and the jet strength but not the profiles. In expressions (3.4*a*,*b*), the velocity is made dimensionless using the vortex core size, a, as a characteristic length and $\Gamma/(2\pi a)$ as characteristic velocity. The constant W_0 characterizes the jet strength and the constant W_{0_0} corresponds to a uniform flow component along the vortex axis. As explained above, such a component is present in helices. It is created by the change of reference frame, because the frame velocity does not correspond to the direction of propagation of the helix (see figure 3). If we take into account only this effect, it is related to the speed V_{frame} of the comoving frame by

$$W_{0_0} = -\frac{\alpha V_{frame}}{\sqrt{1+\alpha^2}}. \tag{3.5}$$

This term is null for vortex rings ($\alpha = 0$), and is $O(\varepsilon \log \varepsilon)$ for helices. Although this term is a higher-order term, it is convenient to introduce it here. We shall see below that it improves the predictions of the axial flow component.

3.2. *Dipolar correction*

The problem at first order provides the main dipolar correction to the axisymmetric vortex. This problem was first solved in a general setting by Callegari & Ting (1978). They showed that the first order corrections satisfy the system

$$\frac{v^{(0)}}{r}(u_\varphi^{(1)} - 2v^{(1)}) + p_r^{(1)} = -[w^{(0)}]^2\cos\varphi, \tag{3.6a}$$

$$ru^{(1)}v_r^{(0)} + v^{(0)}(v_\varphi^{(1)} + u^{(1)}) + p_\varphi^{(1)} = r[w^{(0)}]^2\sin\varphi, \tag{3.6b}$$

$$u^{(1)}w_r^{(0)} + \frac{v^{(0)}}{r}w_\varphi^{(1)} = -[w^{(0)}v^{(0)}]\sin\varphi, \tag{3.6c}$$

$$\frac{1}{r}(ru^{(1)})_r + \frac{1}{r}v_\varphi^{(1)} = -v^{(0)}\sin\varphi. \tag{3.6d}$$

This system possesses a solution of the form

$$u^{(1)} = \hat{u}^{(1)}(r)\sin\varphi = -\frac{\hat{\psi}^{(1)}}{r}\sin\varphi, \tag{3.7a}$$

$$v^{(1)} = \hat{v}^{(1)}(r)\cos\varphi = (-\hat{\psi}_r^{(1)} + rv^{(0)})\cos\varphi, \tag{3.7b}$$

$$w^{(1)} = \hat{w}^{(1)}(r)\cos\varphi = \left(-\frac{w_r^{(0)}}{v^{(0)}}\hat{\psi}^{(1)} + rw^{(0)}\right)\cos\varphi, \tag{3.7c}$$

$$p^{(1)} = \hat{p}^{(1)}(r)\cos\varphi = (-\zeta^{(0)}\hat{\psi}^{(1)} + v^{(0)}\hat{\psi}_r^{(1)} - r[v^{(0)}]^2 - r[w^{(0)}]^2)\cos\varphi, \tag{3.7d}$$

where the streamfunction amplitude $\hat{\psi}^{(1)}(r)$ satisfies

$$\mathscr{L}^{(1)}(\hat{\psi}^{(1)}) = 2r\zeta^{(0)} + v^{(0)} + 2r\frac{w^{(0)}w_r^{(0)}}{v^{(0)}}, \tag{3.8}$$

with the operator $\mathscr{L}^{(k)}$ for $k = 1, 2, \ldots$ defined as

$$\mathscr{L}^{(k)} \equiv \left[\frac{\partial^2}{\partial r^2} + \frac{1}{r}\frac{\partial}{\partial r} - \left(\frac{k^2}{r^2} + \frac{\zeta_r^{(0)}}{v^{(0)}}\right)\right]. \tag{3.9}$$

Using the method of variation of constants, (3.8) can be integrated in closed form as it possesses $v^{(0)}$ as an exact homogeneous solution. If the centre of the local frame is chosen such that the velocity in the $(\boldsymbol{n}, \boldsymbol{b})$ plane vanishes at the origin (up to $O(\varepsilon^2)$), $\hat{\psi}_r^{(1)}(0) = 0$ and $\hat{\psi}^{(1)}(0) = 0$ must be imposed, hence

$$\hat{\psi}^{(1)}(r) = v^{(0)}(r)\int_0^r \frac{\displaystyle\int_0^z v^{(0)}(\eta)\left[2\eta\zeta^{(0)}(\eta) + v^{(0)}(\eta) + 2\eta\frac{w^{(0)}(\eta)w_r^{(0)}(\eta)}{v^{(0)}(\eta)}\right]\eta\,\mathrm{d}\eta}{z[v^{(0)}(z)]^2}\,\mathrm{d}z. \tag{3.10}$$

As explained in Fukumoto & Moffatt (2000), adding a homogeneous solution $c_1 v^{(0)}$ to $\hat{\psi}^{(1)}$ corresponds to a change of frame centre. In the present work, the frame centre has been selected as the stagnation point of the flow, and this corresponds to $c_1 = 0$. As soon as the frame centre is fixed, there are no free parameters: streamfunction, velocity and pressure are given at first order by (3.7*a–d*) and (3.10).

The first-order correction is thus a pure dipolar correction which depends on the local curvature only. This correction is thus identical for a ring, an array of rings, a helix and an array of N helices. It is easy to show that $\hat{\psi}^{(1)}$ expands for large r (Fukumoto & Miyazaki 1991) as follows

$$\hat{\psi}^{(1)} \sim \frac{1}{2}r\log r + rA + O\left(\frac{1}{r}\right), \tag{3.11}$$

with

$$\begin{aligned} A &= \frac{1}{2}\lim_{r\to\infty}\left(\int_0^r \eta(v^{(0)}(\eta))^2\,\mathrm{d}\eta - \log r\right) + \frac{1}{4} - \int_0^\infty \eta((w^{(0)}(\eta))^2 - W_{0_0}^2)\,\mathrm{d}\eta \\ &= \frac{1}{4}(1 - W_0(W_0 + 2W_{0_0}) + \gamma - \log 2) \end{aligned} \tag{3.12}$$

and $\gamma \approx 0.577$ being Euler's constant. As $W_0 W_{0_0}$ is always small, we shall use the approximation $A \approx 0.22 - W_0^2/4$. In figure 4, the streamfunction, $\hat{\psi}^{(1)}/r$ is plotted together with its asymptotic behaviour for the Batchelor vortex for two jet parameters ($W_0 = 0$, $W_0 = 1$) and $W_{0_0} = 0$. When $W_0 = 0$, the dipolar component of the axial velocity follows the simple linear expression $\hat{w}^{(1)}(r) = rW_{0_0}$.

As shown by Fukumoto & Okulov (2005), dipolar corrections are modified by torsion at second order. Thus, rings and helices generate a different dipolar correction only if we consider higher-order terms.

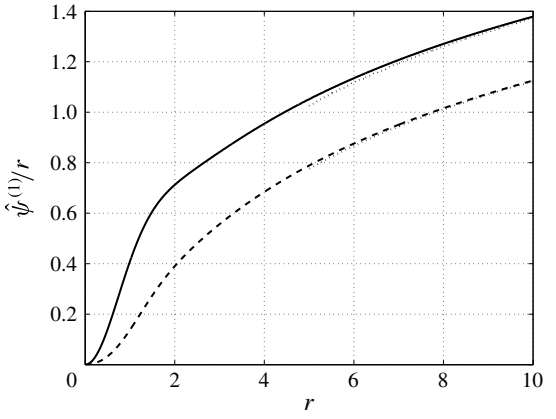

FIGURE 4. Characteristics of the dipolar correction for the Batchelor vortex. $\hat{\psi}^{(1)}/r$ versus r (solid line: $W_0 = 0$; dashed line: $W_0 = 1$. $W_{0_0} = 0$ for both cases) The dotted lines correspond to the asymptotic behaviour (3.11).

3.3. *Quadrupolar correction*

Quadrupolar corrections do not appear at first order but they are generated at second order. At second order, dipolar and monopolar corrections are also generated but we focus here on quadrupolar corrections, as monopolar and dipolar fields were already obtained at lower order. The perturbation equations for the second-order corrections are given by

$$\frac{v^{(0)}}{r}(u_\varphi^{(2)} - 2v^{(2)}) + p_r^{(2)} = \left[\frac{v^{(1)}}{r}(v^{(1)} - u_\varphi^{(1)}) - u^{(1)}u_r^{(1)}\right] - w^{(0)}(2w^{(1)}\cos\varphi + w^{(0)}r\cos^2\varphi), \tag{3.13a}$$

$$ru^{(2)}v_r^{(0)} + v^{(0)}(v_\varphi^{(2)} + u^{(2)}) + p_\varphi^{(2)} = -[ru^{(1)}v_r^{(1)} + v^{(1)}(v_\varphi^{(1)} + u^{(1)})] + rw^{(0)}(2w^{(1)}\sin\varphi + w^{(0)}r\cos\varphi\sin\varphi), \tag{3.13b}$$

$$u^{(2)}w_r^{(0)} + \frac{v^{(0)}}{r}w_\varphi^{(2)} = -\left[u^{(1)}w_r^{(1)} + \frac{v^{(1)}}{r}w_\varphi^{(1)}\right] - v^{(0)}w^{(1)}\sin\varphi + w^{(0)}(u^{(1)}\cos\varphi - v^{(1)}\sin\varphi - rv^{(0)}\cos\varphi\sin\varphi), \tag{3.13c}$$

$$\frac{1}{r}(ru^{(2)})_r + \frac{1}{r}v_\varphi^{(2)} = u^{(1)}\cos\varphi - v^{(1)}\sin\varphi - rv^{(0)}\cos\varphi\sin\varphi. \tag{3.13d}$$

The quadrupolar field satisfying these equations is found to be of the form

$$u_{quad}^{(2)} = \hat{u}^{(2)}(r)\sin 2\varphi = -\frac{2}{r}\hat{\psi}^{(2)}\sin 2\varphi, \tag{3.14a}$$

$$v_{quad}^{(2)} = \hat{v}^{(2)}(r)\cos 2\varphi = (-\hat{\psi}_r^{(2)} + V_F)\cos 2\varphi, \tag{3.14b}$$

$$w_{quad}^{(2)} = \hat{w}^{(2)}(r)\cos 2\varphi = \left(-\frac{w_r^{(0)}}{v^{(0)}}\hat{\psi}^{(2)} + W_F\right)\cos 2\varphi, \tag{3.14c}$$

$$p_{quad}^{(2)} = \hat{p}^{(2)}(r)\cos 2\varphi = (-\zeta^{(0)}\hat{\psi}^{(2)} + v^{(0)}\hat{\psi}_r^{(2)} + P_F)\cos 2\varphi, \tag{3.14d}$$

with

$$V_F = \frac{r^2}{4}(\hat{u}_r^{(1)} + 2v^{(0)}), \tag{3.15a}$$

$$W_F = \frac{r}{4v^{(0)}}\left[-\frac{\hat{w}^{(1)}\hat{v}^{(1)}}{r} + \hat{w}_r^{(1)}\hat{u}^{(1)} + v^{(0)}(\hat{w}^{(1)} + rw^{(0)}) + w^{(0)}(\hat{v}^{(1)} - \hat{u}^{(1)})\right], \tag{3.15b}$$

$$P_F = \frac{r}{4}\hat{u}^{(1)}\hat{v}_r^{(1)} - \frac{\hat{v}^{(1)}}{4}(\hat{v}^{(1)} - \hat{u}^{(1)}) - \frac{r}{2}w^{(0)}\left(\hat{w}^{(1)} + \frac{r}{2}w^{(0)}\right) - v^{(0)}V_F. \tag{3.15c}$$

The streamfunction amplitude $\hat{\psi}^{(2)}$ satisfies

$$\mathscr{L}^{(2)}(\hat{\psi}^{(2)}) = \mathscr{F}, \tag{3.16}$$

with

$$\mathscr{F} = \frac{3rv^{(0)}}{4} - \frac{r\hat{\psi}^{(1)}\zeta_r^{(0)}}{v^{(0)}} - \frac{(\hat{\psi}^{(1)})^2}{4v^{(0)}}\left(\frac{\zeta_r^{(0)}}{v^{(0)}}\right)_r + \frac{r\hat{\psi}^{(1)}}{[v^{(0)}]^2}\left[\frac{w^{(0)}w_r^{(0)}v_r^{(0)}}{v^{(0)}} - (w^{(0)}w_r^{(0)})_r\right]. \tag{3.17}$$

The general solution to (3.16) which is finite at the origin, can be written as

$$\hat{\psi}^{(2)} = S\Psi^{(2)}(r) + \Psi_{NH}^{(2)}(r), \tag{3.18}$$

where $\Psi^{(2)}$ denotes the homogeneous function such that

$$\mathscr{L}^{(2)}(\Psi^{(2)}) = 0, \quad \Psi^{(2)} \underset{r\to 0}{\sim} s_0 r^2, \quad \Psi^{(2)} \underset{r\to+\infty}{\sim} r^2, \tag{3.19a–c}$$

and $\Psi_{NH}^{(2)}$ denotes a particular solution to the non-homogeneous problem (3.16). Finally, S is an arbitrary constant.

It is worth mentioning that another homogeneous solution of (3.13*a–d*) corresponding to a radial velocity proportional to $(2/r)\Psi^{(2)}(r)\cos 2\varphi$ could have been added in principle in (3.14*a*). This solution turns out not to be present for rings and helices, as will be seen in the expressions of the outer solution given in the next section.

The function $\Psi^{(2)}$ describes how a strain field is transmitted within a vortex. It was first introduced by Moffatt *et al.* (1994) for the asymptotic analysis of a vortex in a strain field. Eloy & Le Dizès (1999) showed that $s_0 \approx 2.525$ for a Gaussian vorticity profile. Function $\Psi_{NH}^{(2)}$ (and consequently $\hat{\psi}^{(2)}$) is expected to behave as $3/16r^2\log r$ for large r (see figure 5) because $\mathscr{F} \sim 3/4$ as $r \to +\infty$. Using the method of variation of constants and the fact that $\Psi^{(2)}$ is an exact solution of the homogeneous problem, $\Psi_{NH}^{(2)}$ is given by

$$\Psi_{NH}^{(2)} = \Psi^{(2)}(r)\left[\frac{3}{16}\log r - \int_r^{+\infty}\left(\frac{\int_0^s \eta\mathscr{F}(\eta)\Psi^{(2)}(\eta)\,\mathrm{d}\eta}{s[\Psi^{(2)}]^2} - \frac{3}{16s}\right)\mathrm{d}s\right]. \tag{3.20}$$

The strain rate $S_{NH}^{(2)} = \lim_{r\to 0}\Psi_{NH}^{(2)}/r^2$, which is associated with local curvature effects (it is not present for straight vortices (see, for instance, Le Dizès & Verga 2002)), strongly varies with respect to the jet parameter W_0 (see figure 6). Finally, the function $\Psi^{(2)}$ only depends on $v^{(0)}$ and the function $\Psi_{NH}^{(2)}$ only on $v^{(0)}$ and $w^{(0)}$, that is, they

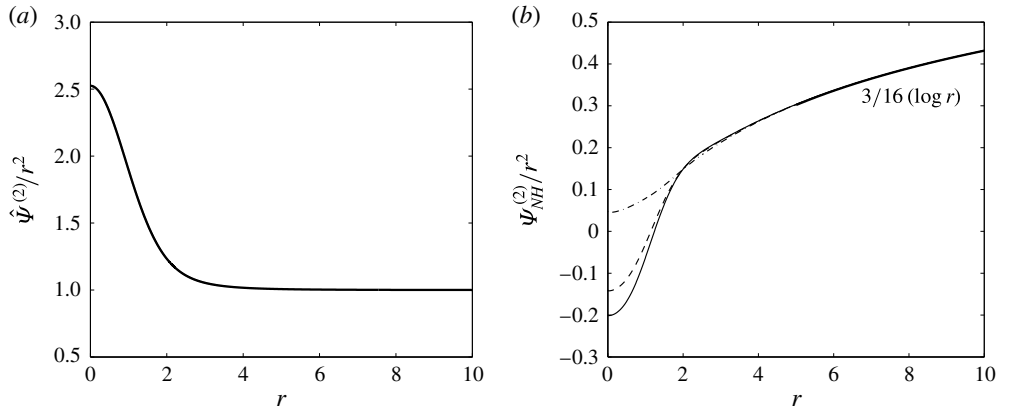

FIGURE 5. Characteristics of the quadrupolar correction for a Batchelor vortex. (*a*) $\Psi^{(2)}/r^2$ versus r; (*b*) $\Psi^{(2)}_{NH}/r^2$ versus r (solid line: $W_0 = 0$, dashed line: $W_0 = 0.4$, dash-dot line: $W_0 = 1$). For all cases, $W_{0_0} = 0$.

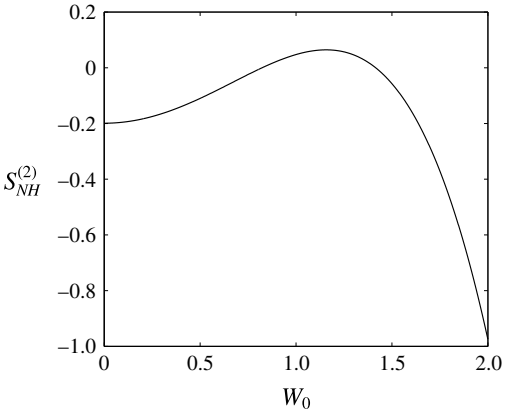

FIGURE 6. Variation of $S^{(2)}_{NH}$ with respect to W_0 for $W_{0_0} = 0$.

only depend on the local properties of the underlying axisymmetrical vortex. These two functions are plotted in figure 5 for the Batchelor vortex for three values of the jet parameter.

The constant S is not determined from the above inner analysis but from matching with an outer solution. It is hence expected to be different for each case; S is actually related to the external strain field experienced by the vortex (see the following section). Contrary to the dipolar correction, the quadrupolar correction is dependent on non-local effects. Yet this dependence comes about through a single constant! Near the origin, the function $\hat{\psi}^{(2)}$ represents a pure strain field

$$\hat{\psi}^{(2)} \sim S^{(2)} r^2, \tag{3.21}$$

where $S^{(2)} = s_0 S + S^{(2)}_{NH}$. The principal directions of this strain field are $\varphi = \pm\pi/4$.

The choice of the frame centre selected at first order does not affect the constant S, but has an impact on the forcing term $\mathscr{F}$, and thus on the function $\Psi^{(2)}_{NH}$. When

$W_0 = 0$, the axial flow component is particularly simple $\hat{w}^{(2)} = r^2 W_{0_0}/2$ and the other velocity components become independent of W_{0_0}.

4. External strain field

The constant S depends on the strain field induced by the background flow. It comes about through an asymptotic matching of the inner solution previously obtained with the outer solution obtained by the Biot–Savart law.

Let us consider the velocity $\boldsymbol{u}^{(out)}$ induced by the vortex system in a reference frame where the system is steady. Such a frame is chosen here as the frame uniformly translating with a velocity $V_{frame}\boldsymbol{e}_z$.

To get the outer solution, we assume that the vorticity is a monopolar field concentrated on the curve $\mathscr{S}$ corresponding to one of the configurations shown in figure 1. The velocity is then such that

$$\boldsymbol{u}^{(out)}(\boldsymbol{x}) = \boldsymbol{u}^{(BS)}(\boldsymbol{x}) - V_{frame}\boldsymbol{e}_z, \quad \text{with } \boldsymbol{u}^{(BS)}(\boldsymbol{x}) = -\frac{1}{4\pi}\int_{\mathscr{S}} \Gamma' \frac{(\boldsymbol{x}-\boldsymbol{x}')\times \boldsymbol{t}'}{|\boldsymbol{x}-\boldsymbol{x}'|^3}\,\mathrm{d}s'. \quad (4.1)$$

All vortices have a constant circulation $\Gamma' = 2\pi$. Note that we do not consider the transverse distribution of vorticity on $\mathscr{S}$ associated with the axial flow within the vortex. Indeed, this vorticity distribution is not expected to contribute to the external flow, as proved by Fukumoto & Miyazaki (1991). We also disregard higher-order corrections to (4.1) corresponding to multipolar vorticity concentration on $\mathscr{S}$; these corrections would be needed to perform a full matching of inner and outer solutions up to $O(\varepsilon^2)$ (see for instance Fukumoto & Moffatt 2000) but are not required for the computation of S. Here, we simply match the quadrupolar field of one component of the velocity field at leading-order only. More precisely, we impose that the local radial velocity of the outer solution possesses a quadrupolar part $u^{(out)}_{quad}$ of the form

$$u^{(out)}_{quad} = u^{(BS)}_{quad} \sim \varepsilon^2[(-2Sr - \tfrac{3}{8}r\log r)\sin 2\varphi] \quad \text{for } 1 \ll r \ll 1/\varepsilon. \quad (4.2)$$

4.1. *A single vortex ring*

The asymptotic description of a single ring was first considered by Widnall & Tsai (1977). It was recently re-examined by Fukumoto & Moffatt (2000) and Fukumoto (2002). Fukumoto & Moffatt (2000) obtained an asymptotic solution up to ε^3 which can be used for the present analysis. Their expression (3.7) of the outer solution in the regime $(1 \ll r \ll R)$ leads to the radial velocity

$$u^{(BS)} \sim \frac{1}{2R}\left(\log\left(\frac{8R}{r}\right) - 1\right)\sin\varphi + \frac{3r}{8R^2}\left(\log\left(\frac{8R}{r}\right) - \frac{4}{3}\right)\sin 2\varphi. \quad (4.3)$$

Since $\varepsilon = 1/R$ for the ring, the matching of their quadrupolar field with the inner quadrupolar part (4.2) requires that

$$S^{Ri} = -\frac{3}{16}\left[\log\left(\frac{8}{\varepsilon}\right) - \frac{4}{3}\right]. \quad (4.4)$$

Note that such a formula could have also been obtained from expression (4.21) of Widnall & Tsai (1977).

4.2. *An array of vortex rings*

The velocity field of an array of vortex rings is equal to the field of a single ring plus the field generated by distant rings. The first contribution has been calculated in the previous section. The contribution from distant rings can be obtained directly from the Biot–Savart integral. The velocity field of the ring placed at position $z = 2\pi n L_z$ can be written using the global cylindrical coordinate system (see appendix A) as

$$v_{n,\rho}^{(BS)}(\rho, z) = -\frac{1}{2}\int_0^{2\pi} \frac{R(z - 2\pi n L_z)\cos s}{(\rho^2 - 2R\rho\cos s + R^2 + (z - 2\pi n L_z)^2)^{3/2}}\,\mathrm{d}s, \tag{4.5a}$$

$$v_{n,z}^{(BS)}(\rho, z) = -\frac{1}{2}\int_0^{2\pi} \frac{R(R^2 - \rho R\cos s + (z - 2\pi n L_z)^2)\cos s}{(\rho^2 - 2R\rho\cos s + R^2 + (z - 2\pi n L_z)^2)^{3/2}}\,\mathrm{d}s. \tag{4.5b}$$

Using the expression for the local radial velocity (see appendix A), one obtains ($L = \alpha = 0$)

$$u(r, \varphi) = -v_\rho\cos\varphi + v_z\sin\varphi \tag{4.6}$$

$$\rho = R - r\cos\varphi, \quad z = r\sin\varphi \tag{4.7a,b}$$

Finally, the dipolar and quadrupolar terms are for $r \ll R$

$$u^{BS} \sim \sum_{n\neq 0}\left[v_{n,z}^{(BS)}(R, 0)\sin\varphi - \frac{r}{2}(\partial_z v_{n,\rho}^{(BS)}(R, 0) + \partial_\rho v_{n,z}^{(BS)}(R, 0))\sin 2\varphi\right]. \tag{4.8}$$

The quadrupolar velocity contribution from distant rings becomes ($\varepsilon = 1/R$)

$$u_{quad}^{BS} \sim -2S^{DRi}\varepsilon^2 r, \quad \text{with } S^{DRi} = \frac{R^2}{2}\sum_{n=1}^{\infty}(\partial_z v_{n,\rho}^{(BS)}(R, 0) + \partial_\rho v_{n,z}^{(BS)}(R, 0)). \tag{4.9}$$

As shown by Levy & Forsdyke (1927), S^{DRi} can also be expressed in terms of the complete elliptic integrals of the first and second kind, $\boldsymbol{K}(Z)$ and $\boldsymbol{E}(Z)$, (Abramowitz & Stegun 1965, p. 590)

$$S^{DRi} = \frac{1}{4}\sum_{n=1}^{\infty}\Lambda_n^{3/2}\left(\left(1 - \frac{4}{n^2\lambda^2}\right)\boldsymbol{E}(\Lambda_n) - \boldsymbol{K}(\Lambda_n)\right), \tag{4.10}$$

with

$$\Lambda_n = \frac{1}{1 + n^2\lambda^2/4}. \tag{4.11}$$

The function S^{DRi} is plotted in figure 7 as a function of the parameter $\lambda = L_z/R$. The constant S for an array of vortex rings is

$$S^{ARi} = S^{DRi} + S^{Ri}. \tag{4.12}$$

Both contributions are negative, and tend to elongate the vortex core along the z direction. In figure 8, the total contribution is plotted as a function of λ for a few values of ε.

Note that because

$$S^{DRi} \sim -\frac{\pi^2}{6\lambda^2} \quad \text{as } \lambda \to 0, \tag{4.13}$$

the complete external strain rate is equal to $S_{ext} \equiv 2S^{DRi}\varepsilon^2 \sim -\pi^2/(3L_z^2)$ which is equal to the external strain rate generated by an array of point vortices of circulation 2π separated by a distance L_z (Lamb 1932).

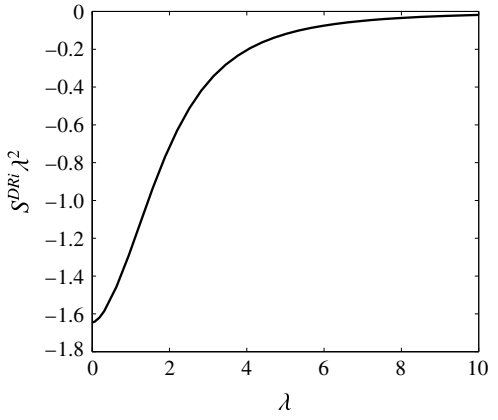

FIGURE 7. Strain rate parameter S^{DRi} generated by distant rings in an array of rings as a function of the aspect ratio $\lambda = L_z/R$.

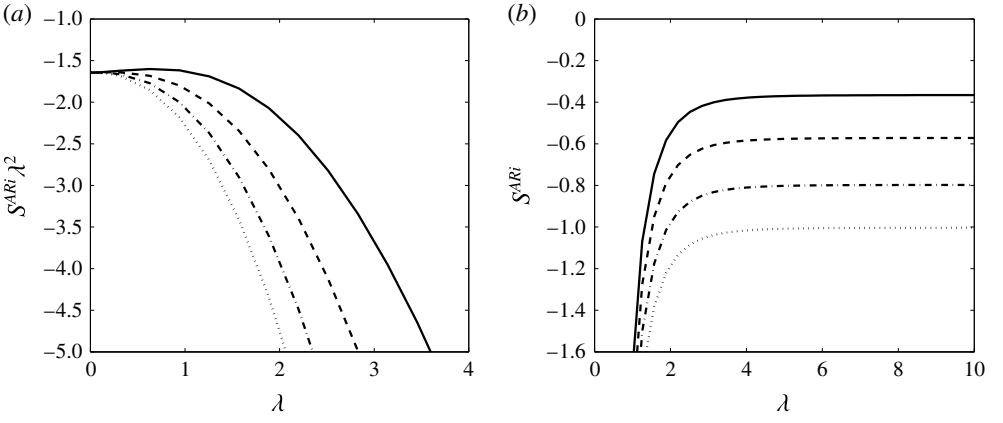

FIGURE 8. Strain rate parameter S^{ARi} for an array of vortex rings as a function of $\lambda = L_z/R$ for various $\varepsilon = a/R$. Solid line: $\varepsilon = 0.33$; dashed line: $\varepsilon = 0.1$; dash-dot line: $\varepsilon = 0.033$; dotted line: $\varepsilon = 0.01$.

4.3. *A single helix*

As shown by Hardin (1982), the velocity field induced by a helical vortex filament can be expressed in cylindrical coordinates for $\rho < R$ (with our normalization) as

$$v_\rho^{(BS)}(\rho, \chi) = \frac{2}{R\alpha^2}\,\mathrm{Im}\left[H_1^{1,1}\left(\frac{\rho}{R\alpha}, \frac{1}{\alpha}, \chi\right)\right], \tag{4.14a}$$

$$v_\phi^{(BS)}(\rho, \chi) = \frac{2}{\rho\alpha}\,\mathrm{Re}\left[H_1^{0,1}\left(\frac{\rho}{R\alpha}, \frac{1}{\alpha}, \chi\right)\right], \tag{4.14b}$$

$$v_z^{(BS)}(\rho, \chi) = \frac{1}{R\alpha} - \frac{2}{R\alpha^2}\,\mathrm{Re}\left[H_1^{0,1}\left(\frac{\rho}{R\alpha}, \frac{1}{\alpha}, \chi\right)\right], \tag{4.14c}$$

where $\chi = \phi - z/L$ and Re[ ] (respectively Im[ ]) indicates the real (respectively imaginary) part of a complex expression, and

$$H_M^{I,J}(x, y, \chi) = \sum_{m=1}^{\infty} m^M I_m^{(I)}(mx) K_m^{(J)}(my) \exp(\mathrm{i}m\chi), \tag{4.15}$$

where we used the notation introduced by Okulov (2004) for the Kapteyn series. $I_m^{(I)}$ and $K_m^{(J)}$ denote the Ith and Jth derivative of modified Bessel functions. Other expressions for the velocity field can be obtained for $\rho > R$, but we only need the above expressions valid for $\rho < R$ to compute the value of S.

The value $\chi = 0$ defines the angular position of the helix. Without restriction, we can consider a local frame centred on the point in cylindrical coordinates $(\rho, \phi, z) = (R, 0, 0)$. The local radial velocity u can be deduced from (4.14*a–c*) using (A 4*a*) and (A 5*a–c*) given in appendix A. We are interested in the expansion of u as r/R goes to zero. As shown by Okulov (2004), it is convenient to isolate the singularity of the Kapteyn series to obtain such an expansion (see appendix B). The derivation, which should be carried up to $O(r/R)^2$ terms, is tedious but straightforward. It can be facilitated by using a symbolic software. The final result is expression (B 12) for u with the following expression for S:

$$\begin{aligned} S^{He} = & -\frac{3}{16}\log\left(\frac{\alpha}{(\alpha^2+1)^{3/2}\varepsilon}\right) - \frac{(\alpha^2+1)^2}{24\alpha^2} - \frac{1}{4}(\alpha^2+1)^2 + \frac{1}{4}\alpha(\alpha^2+1)^{3/2} \\ & + \frac{1}{96}(28\alpha^2+11) + \sum_{m=1}^{\infty} R_m(\alpha), \end{aligned} \tag{4.16}$$

with

$$\begin{aligned} R_m(\alpha) = & \frac{\alpha(\alpha^2+1)^{3/2}}{2} + \frac{3}{16m} - \frac{(1+\alpha^2)^3 m}{2\alpha^2} \\ & + \frac{m^2(\alpha^2+1)^{5/2}}{\alpha^3}\left(-I_{m-1}\left(\frac{m}{\alpha}\right) + \alpha I_m\left(\frac{m}{\alpha}\right)\right)\left(K_{m-1}\left(\frac{m}{\alpha}\right) + \alpha K_m\left(\frac{m}{\alpha}\right)\right) \\ & + m(\alpha^2+1)^{3/2} I_m\left(\frac{m}{\alpha}\right)\left(K_{m-1}\left(\frac{m}{\alpha}\right) + \alpha K_m\left(\frac{m}{\alpha}\right)\right). \end{aligned} \tag{4.17}$$

The function S^{He} is plotted in figure 9 for various values of ε.

Note that when $\alpha \to 0$, we have $S^{He} \sim -1/(24\alpha^2)$, which corresponds to the value (4.13) for an array of rings for small λ since we have the relation $\lambda = 2\pi\alpha$. From figure 9, we can also guess that $S^{He} \sim O(\alpha^2)$ as $\alpha \to \infty$, which implies that the self-external strain of a helix does vanish when its pitch L/R goes to infinity with a fixed a/R.

4.4. *Multiple helices*

When there are several helices, we must add to the previous contribution of a single helix, the contribution from the other distant helices. Expressions (4.14*a–c*) for the velocity field can still be used. For the helix located in the horizontal plane $(0xy)$ at $\phi_k = 2\pi k/N$, we have to change $\chi = \phi - z/L$ into $\chi = (\phi - \phi_k) - z/L$. Summing the contribution from each helix for $k = 1, \ldots, N-1$ and expanding every quantity

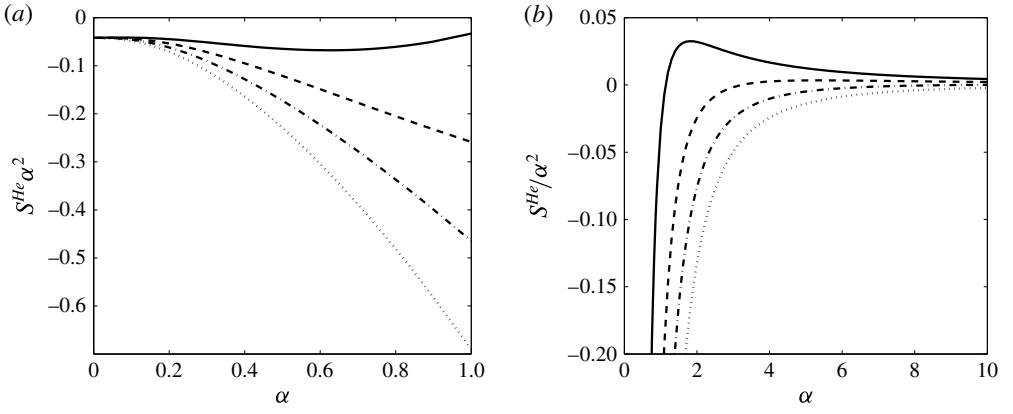

FIGURE 9. Strain rate parameter S^{He} as a function of $\alpha = L/R$ for various ε. Solid line: $\varepsilon = 0.33$; dashed line: $\varepsilon = 0.1$; dash-dot line: $\varepsilon = 0.033$; dotted line: $\varepsilon = 0.01$.

as $r/R \to 0$ leads to expression (B 15) for the local radial velocity (see appendix B) where S is given by

$$S^{DHe} = \frac{3\log(N)}{16} - \frac{(\alpha^2+1)^3(N^2-1)}{24\alpha^2} + \frac{\alpha(\alpha^2+1)^{3/2}(N-1)}{4} + \sum_{m=1}^{\infty} R_m(\alpha)\varrho\left(\frac{m}{N}\right), \tag{4.18}$$

with $R_m(\alpha)$ given by (4.17) and

$$\varrho\left(\frac{m}{N}\right) = \sum_{k=1}^{N-1}\cos\left(2\pi k\frac{m}{N}\right) = \begin{cases} -1 & \frac{m}{N} \notin \mathbb{N}, \\ N-1 & \frac{m}{N} \in \mathbb{N}. \end{cases} \tag{4.19}$$

We obtain for multiple helices $S^{MHe} = S^{He} + S^{DHe}$, that is

$$S^{MHe} = -\frac{3}{16}\log\left(\frac{\alpha}{(\alpha^2+1)^{3/2}N\varepsilon}\right) - \frac{4(\alpha^2+1)^3N^2 + \alpha^2(20\alpha^4+12\alpha^2+9)}{96\alpha^2} + \frac{\alpha(\alpha^2+1)^{3/2}N}{4} + N\sum_{n=1}^{\infty} R_{nN}(\alpha). \tag{4.20}$$

The function S^{MHe} is plotted in figure 10 for $N = 1, 2, 3, 5$ and $\varepsilon = 1$. Plots for other values of ε are obtained by adding $(3/16)\log\varepsilon$ as $S^{MHe}(\varepsilon) = S^{MHe}(1) + (3/16)\log\varepsilon$.

Note that we have

$$S^{MHe} \sim -\frac{N^2}{24\alpha^2} \quad \text{as } \alpha \to 0, \tag{4.21}$$

$$S^{MHe} \sim -\frac{(N-1)(N-5)}{24}\alpha^4 \quad \text{as } \alpha \to \infty. \tag{4.22}$$

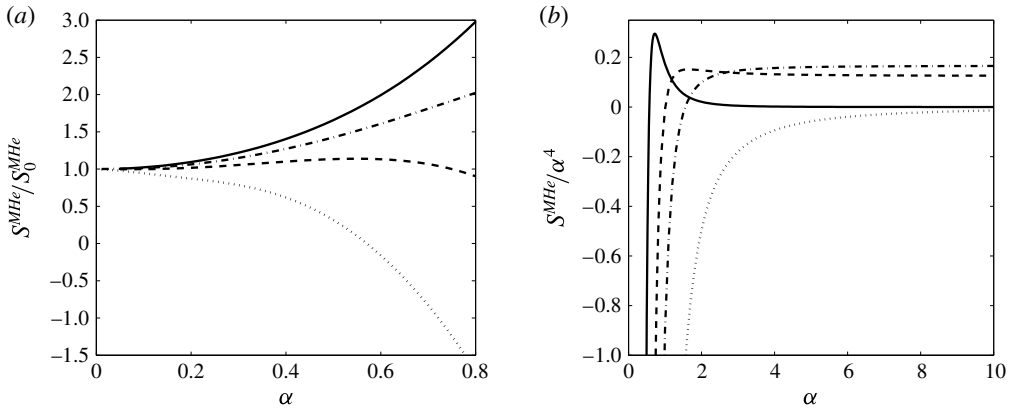

FIGURE 10. Strain rate parameter S^{MHe} versus $\alpha = L/R$ for N helices with $N = 1, 2, 3, 5$ (solid, dash, dash-dot, dotted lines) for $\varepsilon = 1$. (*a*) S^{MHe} is normalized by its expression at the origin $S_0^{MHe} = -N^2/(24\alpha^2)$; (*b*) S^{MHe} is normalized by α^4.

For large α, the problem becomes a configuration of 2-D straight vortices on a polygon. This can be used to check (4.22). For $N = 2$, the calculation is straightforward as the strain field at $(x, y) = (R, 0)$ is due to a vortex of circulation 2π located at $(-R, 0)$. We immediately obtain a strain rate $S_{ext} = 1/(4R^2) = (1/4)\varepsilon^2(1 + \alpha^2)^2 = 2S\varepsilon^2$ which gives $S = (1/8)\alpha^4$ for large α in accordance with (4.22) for $N = 2$.

For large N, we obtain

$$S^{MHe} \sim -\frac{(1+\alpha^2)^3 N^2}{24\alpha^2}, \tag{4.23}$$

which corresponds to the external strain rate generated by an array of straight vortices of circulation 2π and separated by the shortest distance between the helices: $L_z = 2\pi L/(N\sqrt{1+\alpha^2})$.

Note that although S^{MHe} diverges for small and large α, the external strain rate defined by $S_{ext} = 2S^{MHe}\varepsilon^2 = 2S^{MHe}(a/R)^2/(1 + \alpha^2)^2$ remains always small when the core size, a, remains small compared to the shortest distance to the other parts of the vortex structure.

5. Comparison with numerical results

In this section, the asymptotic solution is compared to direct numerical simulations.

5.1. *Simulation of a ring array*

For an array of vortex rings, the pseudo-spectral code developed by Bolnot (2012) is used. This code has been validated and run to analyse the stability of vortex rings with respect to the pairing instability in Bolnot *et al.* (2014). The system is assumed axisymmetric and periodic in the axial direction. The numerical formulation is based on Chebyshev and Fourier decompositions in the radial and axial directions, and on an extrapolation Adams–Bashforth scheme for time evolution. The simulation is initialized by a normalized Gaussian profile for the azimuthal vorticity and velocity

centred at $(\rho, z) = (R_0, 0)$ in a box of axial length L_z with a prescribed jet parameter. At $t = 0$, circulation and core radius of the vortex ring and Reynolds number are fixed to $\Gamma_0 = 2\pi$, $a_0 = 1$ and $Re = \Gamma_0/\nu = 2000$.

After a short relaxation process, the solution reaches a quasi-steady state in the frame moving with the vortex ring (Bolnot *et al.* 2014). The core size and jet parameter have slightly evolved during the relaxation process but are adequately predicted using the viscous expansion factor $\sqrt{1+4t/Re}$ (Bolnot *et al.* 2014). It is this quasi-equilibrium state (frozen at a time t_r) that is compared to the asymptotic solution. In order to agree with the definition used in the asymptotic analysis, the radius R of the ring should correspond to a radial and axial velocity stagnation point. As the plane of symmetry of the solution is fixed in the centre $z = 0$ of the box, the radius R is obtained from the condition $u_z(R, 0) = 0$ which leads to a value slightly different from R_0.

As soon as the centre of the local frame is obtained, the local velocity field (u, v, w) can be computed using (A 4*a–c*), (A 5*a–i*) and (A 1*a–c*). An azimuthal decomposition is then performed to get the monopolar, dipolar and quadrupolar contributions that we compare to the theory.

Figure 11 shows a comparison between asymptotic and DNS results for an array of vortex rings for the parameters $\varepsilon = 0.11$, $\lambda = L_z/R = 3$, $W_0 = 0.1$ and $Re = 2000$. In these figures, we plotted the monopolar, dipolar and quadrupolar contributions of each velocity component in the local frame, using the same normalisation as in the theory. The core size, circulation and jet parameter have been evaluated by comparing the monopolar part (*a*,*d*,*g*) of the numerical velocity fields with the Gaussian model used. It is found that the theoretical profile selected at zero order is appropriate (see comparison figure 11*a*,*d*,*g*). A good agreement between numerical and theoretical curves is also found for all dipolar and quadrupolar components. Other configurations have been tested, and a similar agreement has always been observed. This constitutes a strong validation for both theory and code.

5.2. *Simulation of helices*

The simulations of helix systems have been carried out using the helical code developed in Delbende *et al.* (2012*a*), which implements a generalisation of the vorticity-streamfunction formulation in a circular domain, with finite differences in the radial direction and spectral decomposition along the azimuth. The helical symmetry is explicitly enforced in such a way that the 3-D Navier–Stokes equations are reduced to a 2-D unsteady problem. The code has also been validated and used in Delbende, Rossi & Piton (2012*b*), Delbende, Piton & Rossi (2015).

Similarly to vortex ring simulations, we start the simulation with Gaussian profiles for the axial velocity and axial vorticity around one or several helical curves (see figure 1) with prescribed a_0, R_0, W_0, Γ and L. The Reynolds number is always fixed at $Re = \Gamma/\nu = 10\,000$. After a relaxation process, the system reaches a quasi-equilibrium state in the frame rotating at the rotation rate Ω_{frame} of the helical structure. The rotation rate Ω_{frame} is related to the displacement speed of the helical structure as sketched in figure 3. It can then also be expressed as a function of V_{frame} using $\Omega_{frame} = -V_{frame}/(\alpha R)$.

The difficulty concerning the treatment of the numerical data is the prescription of the local frame. Such a frame is not naturally defined from the DNS, and is obtained here by an iterative procedure. Let us define the helical vorticity ω_B by $\boldsymbol{\omega} \cdot \boldsymbol{e}_B$ where $\boldsymbol{e}_B$ is a unit vector tangent to any helical line (for details see Delbende *et al.* (2012*a*)).

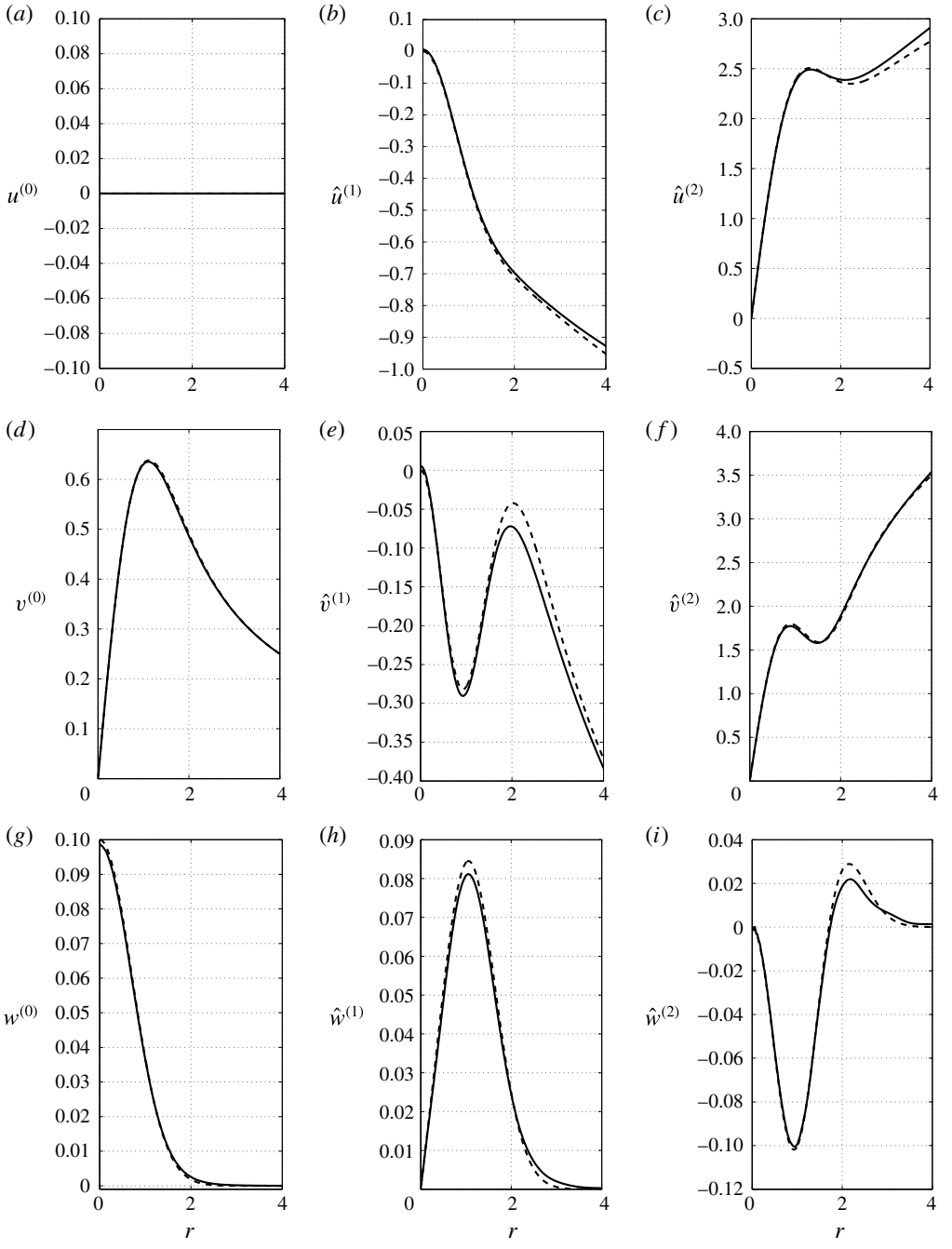

FIGURE 11. Array of swirling vortex rings with jet strength $W_0 = 0.1$, at $L_z/R = 3$, $\varepsilon = 0.11$, $Re = 2000$: comparison between asymptotic results (dashed lines) and DNS results (solid lines). (*a*,*d*,*g*) Monopolar component; (*b*,*e*,*h*): dipolar component; (*c*,*f*,*i*) quadrupolar component. (*a–c*) Radial velocity, (*d–f*) azimuthal velocity, (*g–i*) axial velocity.

This quantity is directly provided by the helical code. First, one finds the position M_0 where the helical vorticity ω_B reaches its maximum in a global horizontal plane. Second, one defines the plane $\Pi_\perp(M_0)$ normal to the local helical vector $\boldsymbol{e}_B(M_0)$ passing through this point M_0. Third, one determines the stagnation point M_1 of the velocity components normal to $\boldsymbol{e}_B(M_0)$ in $\Pi_\perp(M_0)$. At this stagnation point, M_1, the local helical vector $\boldsymbol{e}_B(M_1)$ is oriented in a slightly different direction than $\boldsymbol{e}_B(M_0)$, so a new plane $\Pi_\perp(M_1)$ can be defined in which we can obtain another stagnation point M_2 of the velocity components normal to $\boldsymbol{e}_B(M_1)$ in $\Pi_\perp(M_1)$. This operation is repeated until it has converged to the point that will be the centre of the local frame. In practice, around 100 iterations are necessary. At the end of the process, the stagnation point C has been located, providing a helical line $\mathscr{S}$. The radial coordinate of C defines the value of R. The local frame is such that $\boldsymbol{e}_B(C)$ corresponds to the vector $\boldsymbol{e}_s$ of the theory.

Velocity and vorticity fields are expressed in the cylindrical coordinates attached to this local frame and thereafter Fourier decomposed in the azimuthal direction to obtain the monopolar, dipolar and quadrupolar components. The monopolar components are used to correct the value of the parameters a, Γ and W_0, by fitting axial vorticity and axial velocity with Gaussian profiles, after subtracting the uniform vorticity associated with the rotation of the frame. At the end of this procedure, all theoretical parameters have been obtained and each component can be adequately renormalized for comparison. Note that the frame used in the theory to obtain a steady vortex system is different; it is translating rather than rotating. To express the theoretical results in the rotating frame, one simply subtracts velocity $-V_{frame}\boldsymbol{e}_z + \Omega_{frame}\rho\boldsymbol{e}_\phi$ from the theoretical solution. Using (A 6), this amounts to performing the following modifications on the theoretical fields:

$$v^{(0)} \to v^{(0)} + \varepsilon\sqrt{1+\alpha^2}V_{frame}r, \tag{5.1a}$$

$$w^{(0)} \to w^{(0)} + \frac{\sqrt{1+\alpha^2}}{\alpha}V_{frame}, \tag{5.1b}$$

$$w^{(1)} \to w^{(1)} - \frac{\sqrt{1+\alpha^2}}{\alpha}V_{frame}r. \tag{5.1c}$$

Since V_{frame} is $O(\varepsilon\log\varepsilon)$ for helices, these changes are higher-order terms. Nevertheless, it is convenient to introduce them here because they improve the predictions of the axial flow component, as shown below.

In figure 12 (respectively figure 13), theoretical and numerical results are compared for a single helix with axial flow $W_0 = 0.54$ (respectively for a system of two helices without axial jet $W_0 = 0$). For radial and azimuthal velocity components, a fair agreement is found between theory and DNS results. Despite a smaller value of ε, the agreement is found to be less convincing than for an array of rings. It is also seen that the change (5.1*a–c*) of reference frame has to be taken into account. However, a small mismatch between DNS and theory remains for the monopolar component. This is probably at the origin of the deteriorated agreement for the dipolar and quadrupolar components (see bottom figures in figures 12 and 13).

As for the ring arrays, other configurations have been tested for helical vortex systems and we always observed a good agreement with the asymptotic theory. The values obtained from the numerical simulations for the internal strain rate $S^{(2)}$ and for the frame rotation rate Ω_{frame} have also been compared to the theory and we have systematically found a good agreement. This provides a validation of expressions (4.20) and (B 17) for the external strain field and translation speed of multiple helices.

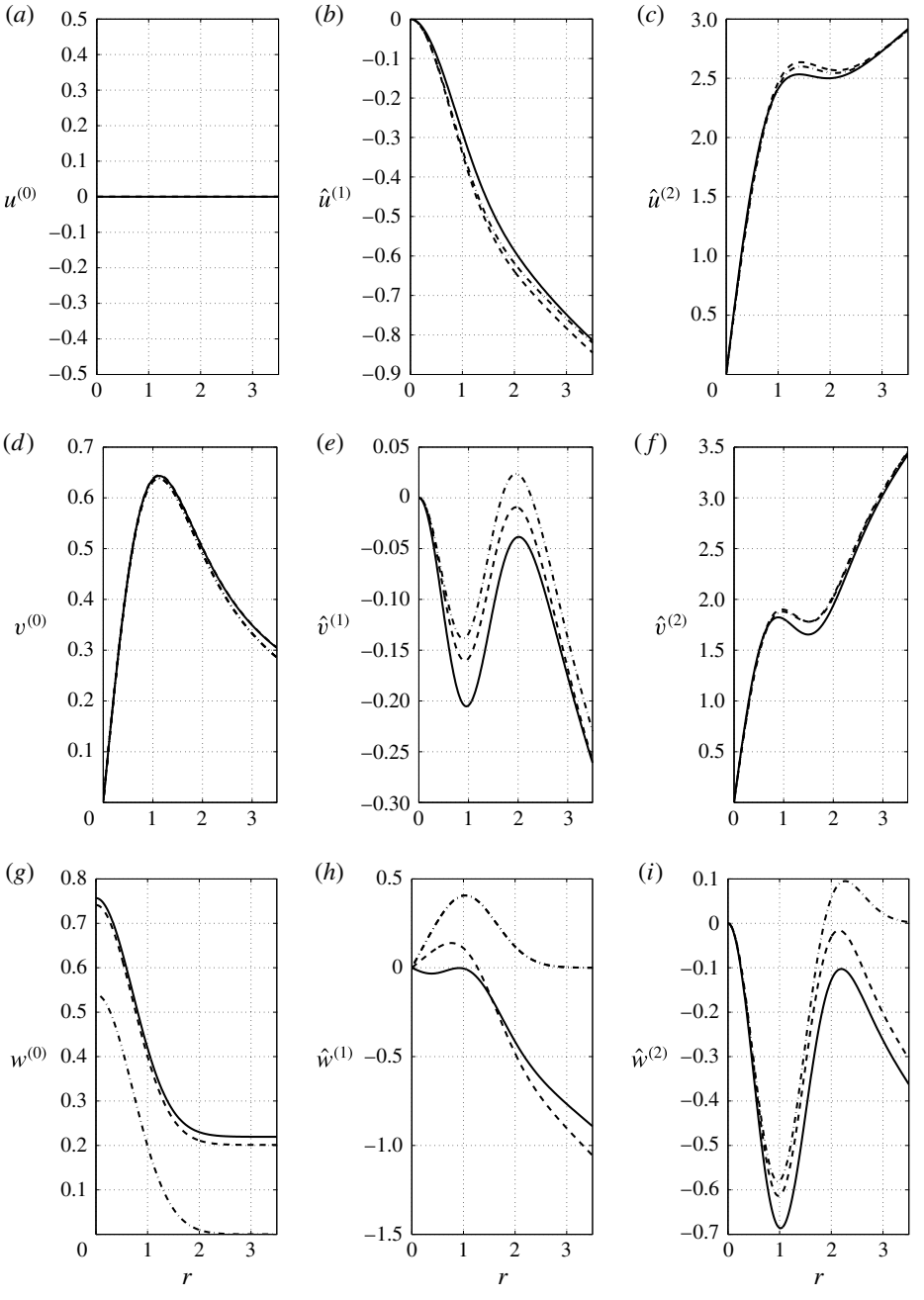

FIGURE 12. Single helix with $W_0 = 0.54$, $L/R = 0.5$, $\varepsilon = 0.045$, $Re = 10^4$: comparison between asymptotic (dashed lines) and DNS (solid lines). (*a*,*d*,*g*) Monopolar component; (*b*,*e*,*h*) dipolar component; (*c*,*f*,*i*) quadrupolar component. (*a–c*) Radial velocity, (*d–f*) azimuthal velocity, (*g–i*) axial velocity. The dash-dotted lines correspond to the theory without taking into account the effect of the change of frame ($W_{0_0} = 0$). For these parameters, the theory gives $\Omega_{frame} = -0.0120$ and $S = -0.6341$, which gives a strain rate in the vortex centre $S^{(2)} = -1.699$ (defined in (3.21)). The numerical values are $\Omega_{frame} = -0.0110$ and $S^{(2)} = -1.803$.

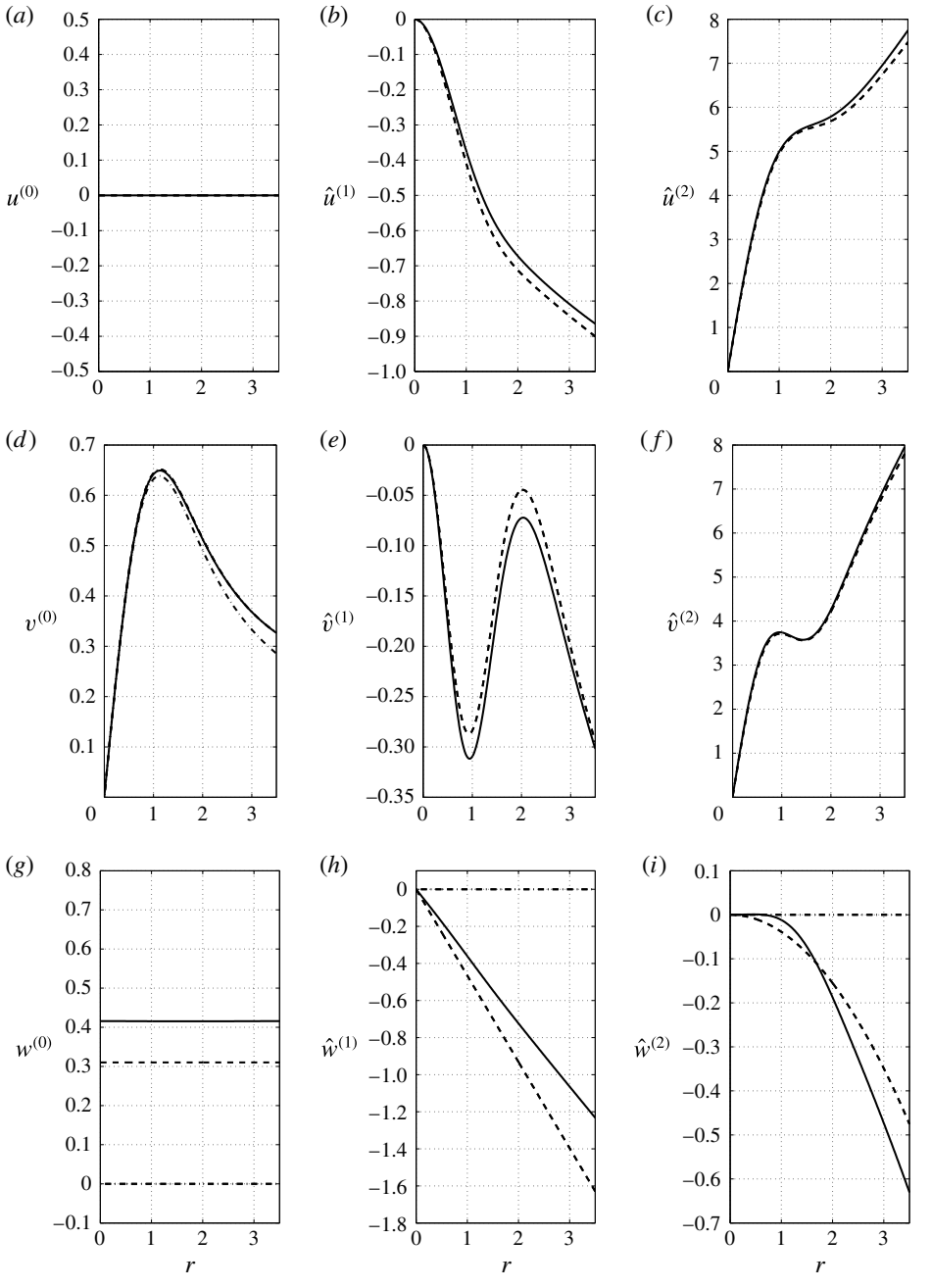

FIGURE 13. System of two helical vortices with $W_0 = 0$, $L/R = 0.5$, $\varepsilon = 0.06$, $Re = 10^4$: comparison between asymptotic (dashed lines) and DNS (solid lines). (*a*,*d*,*g*) Monopolar component; (*b*,*e*,*h*) dipolar component; (*c*,*f*,*i*) quadrupolar component. (*a–c*) Radial velocity, (*d–f*) azimuthal velocity, (*g–i*) axial velocity. The dash-dotted lines correspond to the theory without taking into account the effect of the change of frame ($W_{0_0} = 0$). For these parameters, the theory predicts $\Omega_{frame} = -0.0258$ and $S = -1.2832$, which gives a strain rate in the centre $S^{(2)} = -3.441$ (defined in (3.21)). The numerical values are $\Omega_{frame} = -0.0261$ and $S^{(2)} = -3.496$.

6. Conclusions

We analysed the internal structure of vortex rings and helical vortices showing that they can be described using an asymptotic theory where the core size is considered small compared to the other scales of the vortex structure. At leading order, the vortex structure was assumed locally an axisymmetric vortex with axial flow. The asymptotic theory was used to determine dipolar and quadrupolar corrections associated with this structure. It was shown that dipolar corrections which appear at first order depend in a dominant way on the local curvature of the vortex. As a consequence, we expect rings, arrays of rings, helices and multiples helices to all exhibit the same dipolar correction if they possess the same curvature. We also computed the quadrupolar corrections which appear at second order. Contrary to the dipolar corrections, such corrections depend on the global geometry. To be more precise, quadrupolar corrections are composed of a contribution which depends on the local curvature and a non-local contribution associated with the strain field generated by distant part of the vortex structure. The non-local contribution has been calculated for a vortex ring, an array of rings, a helix and multiple helices by considering the flow field obtained from Biot–Savart law for vortex filaments.

The asymptotic results have been compared to numerical solutions obtained by DNS for both rings and helices. A good agreement has been observed for rings. For helices, a fair agreement has also been demonstrated. In practice, this case is more involved because of the necessity to define a plane orthogonal to the vortex core structure.

The present results are important to model the short-wavelength instabilities that can develop in rings or helices. Both dipolar and quadrupolar correction terms are expected to couple modes of the underlying vortex and be a source of instability. The dipolar correction term is known to be responsible of the so-called curvature instability. This instability has been theoretically predicted for rings (Hattori & Fukumoto 2003; Fukumoto & Hattori 2005) and helices (Hattori & Fukumoto 2009, 2014). However, the analysis has only been performed for particular vortices with uniform vorticity. It would be interesting to extend the analysis to more realistic vortices such as those considered in the present study. The quadrupolar correction is associated with the so-called elliptic instability (see for instance Kerswell 2002). Widnall & Tsai (1977) provided a growth rate estimate for the elliptic instability in a single ring with a Rankine vorticity profile. No person however has so far provided any prediction for helices or rings with a realistic vorticity profile. Yet, we expect this instability to be present as the quadrupolar field contained a strain field part which is also present in straight vortices. An interesting study would then be to compute the effects of the additional quadrupolar field which is generated by curvature.

Both curvature and elliptic instabilities are also expected to be strongly affected by the presence of axial flow, as this parameter modifies the form of vortex modes involved in the instabilities (Lacaze, Ryan & Le Dizès 2007; Roy *et al.* 2011). We suspect that this parameter is crucial to an understanding of the competition between both instabilities and associate recent observations in helices (Leweke *et al.* 2014) with one instability or another.

Acknowledgements

This work received support from the French Agence Nationale de la Recherche under the A*MIDEX grant ANR-11-IDEX-0001-02, the LABEX MEC project ANR-11-LABX-0092 and the ANR HELIX project ANR-12-BS09-0023-01. HPC resources from GENCI–IDRIS (grant 2015-2a1386) are also acknowledged.

Appendix A. Change of coordinate systems

In this section, we provide the formulae which can be used to obtain the velocity field in the local frame from its expression in the global cylindrical frame. Consider a point of coordinates (ρ, ϕ, z) in the global cylindrical coordinate system and assume that this point has the coordinates (r, φ, s) in the local frame defined by (2.1) and (2.3) centred on the point $C(s)$ of cylindrical coordinates $(R, \phi_0, L\phi_0)$ (see figure 2). We obtain the following relation between the coordinates:

$$\rho^2 = (R - r\cos\varphi)^2 + \frac{\alpha^2}{1+\alpha^2} r^2 \sin^2\varphi, \tag{A 1a}$$

$$\rho \sin\phi = (R - r\cos\varphi)\sin\phi_0 - \frac{\alpha}{\sqrt{1+\alpha^2}} r \sin\varphi \cos\phi_0, \tag{A 1b}$$

$$z = L\phi_0 + \frac{1}{\sqrt{1+\alpha^2}} r \sin\varphi, \tag{A 1c}$$

$$s = \phi_0 \sqrt{R^2 + L^2}. \tag{A 1d}$$

If the velocity field can be written in the global cylindrical frame as

$$\boldsymbol{V} = \boldsymbol{V}(\rho, \phi, z) = v_\rho \boldsymbol{e}_\rho + v_\phi \boldsymbol{e}_\phi + v_z \boldsymbol{e}_z \tag{A 2}$$

and

$$\boldsymbol{V} = u\boldsymbol{e}_r + v\boldsymbol{e}_\varphi + w\boldsymbol{e}_s \tag{A 3}$$

in the local frame, we derive the relation between (u, v, w) and (v_ρ, v_ϕ, v_z):

$$u(r, \varphi, s) = v_\rho(\rho, \phi, z)\boldsymbol{e}_r \cdot \boldsymbol{e}_\rho + v_\phi(\rho, \phi, z)\boldsymbol{e}_r \cdot \boldsymbol{e}_\phi + v_z(\rho, \phi, z)\boldsymbol{e}_r \cdot \boldsymbol{e}_z, \tag{A 4a}$$

$$v(r, \varphi, s) = v_\rho(\rho, \phi, z)\boldsymbol{e}_\varphi \cdot \boldsymbol{e}_\rho + v_\phi(\rho, \phi, z)\boldsymbol{e}_\varphi \cdot \boldsymbol{e}_\phi + v_z(\rho, \phi, z)\boldsymbol{e}_\varphi \cdot \boldsymbol{e}_z, \tag{A 4b}$$

$$w(r, \varphi, s) = v_\rho(\rho, \phi, z)\boldsymbol{e}_s \cdot \boldsymbol{e}_\rho + v_\phi(\rho, \phi, z)\boldsymbol{e}_s \cdot \boldsymbol{e}_\phi + v_z(\rho, \phi, z)\boldsymbol{e}_s \cdot \boldsymbol{e}_z, \tag{A 4c}$$

where

$$\boldsymbol{e}_r \cdot \boldsymbol{e}_\rho = -\left(\frac{R}{\rho} - \frac{r}{\rho}\cos\varphi\right)\cos\varphi + \frac{\alpha^2}{(1+\alpha^2)}\frac{r}{\rho}\sin^2\varphi, \tag{A 5a}$$

$$\boldsymbol{e}_r \cdot \boldsymbol{e}_\phi = -\frac{\alpha}{\sqrt{1+\alpha^2}}\frac{R}{\rho}\sin\varphi, \tag{A 5b}$$

$$\boldsymbol{e}_r \cdot \boldsymbol{e}_z = \frac{1}{\sqrt{1+\alpha^2}}\sin\varphi, \tag{A 5c}$$

$$\boldsymbol{e}_\varphi \cdot \boldsymbol{e}_\rho = \left(\frac{R}{\rho} - \frac{r}{\rho}\cos\varphi\right)\sin\varphi + \frac{\alpha^2}{(1+\alpha^2)}\frac{r}{\rho}\sin\varphi\cos\varphi, \tag{A 5d}$$

$$\boldsymbol{e}_\varphi \cdot \boldsymbol{e}_\phi = \frac{\alpha}{\sqrt{1+\alpha^2}}\left(\frac{r}{\rho} - \frac{R}{\rho}\cos\varphi\right), \tag{A 5e}$$

$$\boldsymbol{e}_\varphi \cdot \boldsymbol{e}_z = \frac{1}{\sqrt{1+\alpha^2}}\cos\varphi, \tag{A 5f}$$

$$\boldsymbol{e}_s \cdot \boldsymbol{e}_\rho = -\frac{\alpha}{(1+\alpha^2)}\frac{r}{\rho}\sin\varphi, \tag{A 5g}$$

$$\boldsymbol{e}_s \cdot \boldsymbol{e}_\phi = \frac{1}{\sqrt{1+\alpha^2}}\left(\frac{R}{\rho} - \frac{r}{\rho}\cos\varphi\right), \tag{A 5h}$$

$$\boldsymbol{e}_s \cdot \boldsymbol{e}_z = \frac{\alpha}{\sqrt{1+\alpha^2}}. \tag{A 5i}$$

These expressions can be used to express in the local frame with the local coordinates the vector $\boldsymbol{U} = -V_{frame}\boldsymbol{e}_z + \Omega_{frame}\rho\boldsymbol{e}_\phi$ associated with the change of frame in § 5.2. Using $\Omega_{frame} = -V_{frame}/(\alpha R)$, we obtain

$$\boldsymbol{U} = V_{frame}\left(-\frac{r}{R\sqrt{1+\alpha^2}}\boldsymbol{e}_\varphi + \left(-\frac{\sqrt{1+\alpha^2}}{\alpha} + \frac{r\cos\varphi}{R\alpha\sqrt{1+\alpha^2}}\right)\boldsymbol{e}_s\right). \tag{A 6}$$

Appendix B. Inner expansion of Hardin solution for helices

To derive the inner expansion of Hardin solution, it is convenient to isolate the singularity of the Kapteyn series using the technique introduced by Okulov (2004). We have in particular used the expressions (valid for $\rho < R$) given by Fukumoto & Okulov (2005):

$$v_\rho^{(BS)} = \frac{2}{R\alpha^2}\mathrm{Im}\left[\lambda^{1,1}\left(\frac{\mathrm{e}^{\xi+\mathrm{i}\chi}}{1-\mathrm{e}^{\xi+\mathrm{i}\chi}} + \alpha^{1,1}\log(1-\mathrm{e}^{\xi+\mathrm{i}\chi}) + \beta^{1,1}\mathrm{Li}_2(\mathrm{e}^{\xi+\mathrm{i}\chi})\right) + R_1^{1,1}\right], \tag{B 1a}$$

$$v_\phi^{(BS)} = \frac{2}{\rho\alpha}\mathrm{Re}\left[\lambda^{0,1}\left(\frac{\mathrm{e}^{\xi+\mathrm{i}\chi}}{1-\mathrm{e}^{\xi+\mathrm{i}\chi}} + \alpha^{0,1}\log(1-\mathrm{e}^{\xi+\mathrm{i}\chi}) + \beta^{0,1}\mathrm{Li}_2(\mathrm{e}^{\xi+\mathrm{i}\chi})\right) + R_1^{0,1}\right], \tag{B 1b}$$

$$v_z^{(BS)} = \frac{1}{2\alpha} - \frac{2}{R\alpha^2}\mathrm{Re}\left[\lambda^{0,1}\left(\frac{\mathrm{e}^{\xi+\mathrm{i}\chi}}{1-\mathrm{e}^{\xi+\mathrm{i}\chi}} + \alpha^{0,1}\log(1-\mathrm{e}^{\xi+\mathrm{i}\chi}) + \beta^{0,1}\mathrm{Li}_2(\mathrm{e}^{\xi+\mathrm{i}\chi})\right) + R_1^{0,1}\right], \tag{B 1c}$$

where

$$\chi = \phi - z/(R\alpha), \quad \mathrm{e}^\xi = \frac{x(1+\sqrt{1+y^2})\exp(\sqrt{1+x^2})}{y(1+\sqrt{1+x^2})\exp(\sqrt{1+y^2})}, \tag{B 2a,b}$$

$$\lambda^{1,1} = -\frac{((1+x^2)(1+y^2))^{1/4}}{2xy}, \quad \lambda^{0,1} = -\frac{1}{2y}\left(\frac{1+y^2}{1+x^2}\right)^{1/4}, \tag{B 3a,b}$$

$$\alpha^{1,1} = \upsilon_1(t_x) - \upsilon_1(t_y), \quad \beta^{1,1} = \upsilon_2(t_x) + \upsilon_2(t_y) - \upsilon_1(t_x)\upsilon_1(t_y), \tag{B 4a,b}$$

$$\alpha^{0,1} = \vartheta_1(t_x) - \upsilon_1(t_y), \quad \beta^{0,1} = \vartheta_2(t_x) + \upsilon_2(t_y) - \vartheta_1(t_x)\upsilon_1(t_y), \tag{B 4c,d}$$

with

$$x = \frac{\rho}{R\alpha}, \quad y = \frac{1}{\alpha}, \quad t_x = \frac{1}{\sqrt{1+x^2}}, \quad t_y = \frac{1}{\sqrt{1+y^2}}, \tag{B 5a–d}$$

and

$$\upsilon_1(t) = (-9t + 7t^3)/24, \tag{B.6a}$$

$$\vartheta_1(t) = (3t - 5t^3)/24, \tag{B.6b}$$

$$\upsilon_2(t) = (-135t^2 + 594t^4 - 455t^6)/1152, \tag{B.6c}$$

$$\vartheta_2(t) = (81t^2 - 462t^4 + 385t^6)/1152. \tag{B.6d}$$

The functions $R_1^{1,1}$ and $R_1^{0,1}$ are defined by

$$R_1^{1,1} = \sum_{m=1}^{\infty} ri_m^{1,1}(x, y)\mathrm{e}^{\mathrm{i}m\chi}, \quad R_1^{0,1} = \sum_{m=1}^{\infty} ri_m^{0,1}(x, y)\mathrm{e}^{\mathrm{i}m\chi}, \tag{B 7a,b}$$

with

$$ri_m^{1,1}(x, y) = mI_m'(mx)K_m'(my) - \lambda^{1,1}\mathrm{e}^{m\xi}\left(1 + \frac{\alpha^{1,1}}{m} + \frac{\beta^{1,1}}{m^2}\right), \tag{B.8a}$$

$$ri_m^{0,1}(x, y) = mI_m(mx)K_m'(my) - \lambda^{0,1}\mathrm{e}^{m\xi}\left(1 + \frac{\alpha^{0,1}}{m} + \frac{\beta^{0,1}}{m^2}\right). \tag{B.8b}$$

An expression for u in terms of the local coordinates is obtained using (A 4*a*) and (A 1*a–c*) with $\phi_0 = 0$. Expanding all the quantities as $r/R \to 0$, we find an expression for a single helix of the form

$$u^{(BS)} \sim [C^{He} - \tfrac{1}{2}\log r]\varepsilon \sin\varphi + [-2S^{He} - \tfrac{3}{8}\log r]\varepsilon^2 r \sin 2\varphi, \tag{B.9}$$

where S^{He} is given by (4.16) and

$$C^{He} = \frac{1 - \alpha^4 + \alpha^3\sqrt{1+\alpha^2}}{2\alpha\sqrt{1+\alpha^2}} + \frac{1}{2}\log\left(\frac{\alpha}{\varepsilon(1+\alpha^2)^{3/2}}\right) + \sum_{m=1}^{\infty} c_m(\alpha), \tag{B.10}$$

with

$$c_m(\alpha) = -\frac{(1+\alpha^2)^{3/2}}{\alpha}\left(\frac{2m}{\alpha}I_m\left(\frac{m}{\alpha}\right)K_m'\left(\frac{m}{\alpha}\right) + 1\right) - \frac{1}{2m}. \tag{B.11}$$

Both $R_m(\alpha)$ and $c_m(\alpha)$ are $O(1/m^3)$ for large m, which guarantees that the sums in (4.16) and (B 10) are absolutely convergent.

If we now add the contribution from the displacement of the frame (which is $-V_{frame}^{He}\boldsymbol{e}_z$) we obtain from (4.1) for a single helix

$$u^{(out)} \sim \left[-\frac{V_{frame}^{He}}{\sqrt{1+\alpha^2}} + C^{He} - \frac{1}{2}\log r\right]\varepsilon \sin\varphi + \left[-2S^{He} - \frac{3}{8}\log r\right]\varepsilon^2 r \sin 2\varphi. \tag{B.12}$$

The matching of this expression with the inner expansions provides the strain rate S^{He} and the frame velocity V_{frame}^{He}:

$$V_{frame}^{He} = \sqrt{1+\alpha^2}(C^{He} + A)\varepsilon, \tag{B.13}$$

where A is defined by (3.12). This expression is analogue to an expression already given in Alekseenko *et al.* (2007), p. 250.

The velocity field induced by the distant helices is obtained by summing the $N-1$ contributions taken at $\phi_k = 2\pi k/N$, $k = 1, \ldots, N-1$. There are many simplifications thanks to the relations

$$\sum_{k=1}^{N-1} \frac{\exp(\mathrm{i}\phi_k)}{1-\exp(\mathrm{i}\phi_k)} = \frac{1-N}{2}, \tag{B.14a}$$

$$\sum_{k=1}^{N-1} \log(1-\exp(\mathrm{i}\phi_k)) = \log N, \tag{B.14b}$$

$$\sum_{k=1}^{N-1} \mathrm{Li}_2(\exp(\mathrm{i}\phi_k)) = \frac{\pi^2}{6}\frac{1-N}{N}. \tag{B.14c}$$

After a long but straightforward calculation, we obtain for the contribution from distant helices

$$u^{(BS)} \sim C^{DHe}\varepsilon \sin\varphi - 2S^{DHe}\varepsilon^2 r \sin 2\varphi, \tag{B.15}$$

where S^{DHe} is given by (4.18) and

$$C^{DHe} = -\frac{\sqrt{1+\alpha^2}(\alpha^2-1)(N-1)}{2\alpha} - \frac{1}{2}\log N + \sum_{m=1}^{\infty} c_m(\alpha)\varrho\left(\frac{m}{N}\right), \tag{B.16}$$

with $\varrho(x)$ defined in (4.19).

The velocity field obtained by multiple helices is the sum of the contributions from a single helix and distant helices. From the complete matching of the dipolar component, we obtain using (B 12) and (B 15), an expression for the velocity V^{MHe}_{frame} of the frame for multiple helices:

$$V^{MHe}_{frame} = \sqrt{1+\alpha^2}(C^{MHe} + A)\varepsilon, \tag{B.17}$$

where $C^{MHe} = C^{He} + C^{DHe}$ reduces to

$$C^{MHe} = \frac{\alpha^2}{2} - \frac{\sqrt{1+\alpha^2}(\alpha^2-1)N}{2\alpha} + \frac{1}{2}\log\left(\frac{\alpha}{\varepsilon(1+\alpha^2)^{3/2}N}\right) + N\sum_{k=1}^{\infty} c_{Nk}(\alpha). \tag{B.18}$$

It is this expression of V_{frame}, with $A \approx 0.22 - W_0^2/4$ which has been used in expression (3.5) for W_{0_0} and in (5.1*a–c*).

Note finally that the expressions (B 9) and (B 15), and (4.3) and (4.8) for rings, contain no $\cos 2\phi$ terms. This property validates the hypothesis made in § 3.3 that there is no homogeneous solution proportional to $\cos 2\phi$ in the inner expression (3.14*a*) of the quadrupolar contribution to the radial velocity.

REFERENCES

ABRAMOWITZ, M. & STEGUN, I. A. 1965 *Handbook of Mathematical Functions*. Dover.

ALEKSEENKO, S. V., KUIBIN, P. A. & OKULOV, V. L. 2007 *Theory of Concentrated Vortices: An Introduction*. Springer.

BOERSMA, J. & WOOD, D. H. 1999 On the self-induced motion of a helical vortex. *J. Fluid Mech.* **384**, 263–280.

BOLNOT, H. 2012 Instabilités des tourbillons hélicoïdaux: application au sillage des rotors. PhD thesis, Aix Marseille University.

BOLNOT, H., LE DIZÈS, S. & LEWEKE, T. 2014 Spatio-temporal development of the pairing instability in an infinite array of vortex rings. *Fluid Dyn. Res.* **46**, 061405.

CALLEGARI, A. J. & TING, L. 1978 Motion of a curved vortex filament with decaying vortical core and axial velocity. *SIAM J. Appl. Maths* **35**, 148–175.

DELBENDE, I., PITON, B. & ROSSI, M. 2015 Merging of two helical vortices. *Eur. J. Mech.* (B/*Fluids)* **49**, 363–372.

DELBENDE, I., ROSSI, M. & DAUBE, O. 2012*a* DNS of flows with helical symmetry. *J. Theor. Comput. Fluid Dyn.* **26**, 141–160.

DELBENDE, I., ROSSI, M. & PITON, B. 2012*b* Direct numerical simulation of helical vortices. *Intl J. Engng Systems Model. Simul.* **4**, 94–101.

ELOY, C. & LE DIZÈS, S. 1999 Three-dimensional instability of Burgers and Lamb-Oseen vortices in a strain field. *J. Fluid Mech.* **378**, 145–166.

FUKUMOTO, Y. 2002 Higher-order asymptotic theory for the velocity field induced by an inviscid vortex ring. *Fluid Dyn. Res.* **30**, 67–95.

FUKUMOTO, Y. & HATTORI, Y. 2005 Curvature instability of a vortex ring. *J. Fluid Mech.* **526**, 77–115.

FUKUMOTO, Y. & MIYAZAKI, T. 1991 Three-dimensional distorsions of a vortex filament with axial velocity. *J. Fluid Mech.* **222**, 369–416.

FUKUMOTO, Y. & MOFFATT, H. K. 2000 Motion and expansion of a viscous vortex ring. Part 1. A higher-order asymptotic formula for the velocity. *J. Fluid Mech.* **417**, 1–45.

FUKUMOTO, Y. & OKULOV, V. L. 2005 The velocity induced by a helical vortex tube. *Phys. Fluids* **17**, 107101.

HARDIN, J. C. 1982 The velocity field induced by a helical vortex filament. *Phys. Fluids* **25** (11), 1949–1952.

HATTORI, Y. & FUKUMOTO, Y. 2003 Short-wavelength stability analysis of thin vortex rings. *Phys. Fluids* **15**, 3151–3163.

HATTORI, Y. & FUKUMOTO, Y. 2009 Short-wavelength stability analysis of a helical vortex tube. *Phys. Fluids* **21**, 014104.

HATTORI, Y. & FUKUMOTO, Y. 2014 Modal stability analysis of a helical vortex tube with axial flow. *J. Fluid Mech.* **738**, 222–249.

KERSWELL, R. R. 2002 Elliptical instability. *Annu. Rev. Fluid Mech.* **34**, 83–113.

KUIBIN, P. A. & OKULOV, V. L. 1998 Self-induced motion and asymptotic expansion of the velocity field in the vicinity of a helical vortex filament. *Phys. Fluids* **10**, 607–614.

LACAZE, L., RYAN, K. & LE DIZÈS, S. 2007 Elliptic instability in a strained batchelor vortex. *J. Fluid Mech.* **577**, 341–361.

LAMB, H. 1932 *Hydrodynamics*, 6th edn. Cambridge University Press.

LE DIZÈS, S. & VERGA, A. 2002 Viscous interaction of two co-rotating vortices before merging. *J. Fluid Mech.* **467**, 389–410.

LEVY, H. & FORSDYKE, A. G. 1927 The stability of an infinite system of circular vortices. *Proc. R. Soc. Lond.* A **114**, 594–604.

LEWEKE, T., QUARANTA, H. U., BOLNOT, H., BLANCO-RODRIGUEZ, F. J. & LE DIZÈS, S. 2014 Long- and short-wave instabilities in helical vortices. *J. Phys.: Conf. Ser.* **524**, 012154.

MOFFATT, H. K., KIDA, S. & OHKITANI, K. 1994 Stretched vortices – the sinews of turbulence; large-Reynolds-number asymptotics. *J. Fluid Mech.* **259**, 241–264.

MOORE, D. W. & SAFFMAN, P. G. 1972 The motion of a vortex filament with axial flow. *Phil. Trans. R. Soc. Lond.* A **272**, 403–429.

OKULOV, V. L. 2004 On the stability of multiple helical vortices. *J. Fluid Mech.* **521**, 319–342.

RICCA, R. L. 1994 The effect of torsion on the motion of a helical vortex filament. *J. Fluid Mech.* **273**, 241–259.

ROY, C., LEWEKE, T., THOMPSON, M. C. & HOURIGAN, K. 2011 Experiments on the elliptic instability in vortex pairs with axial core flow. *J. Fluid Mech.* **677**, 383–416.

SAFFMAN, P. G. 1992 *Vortex Dynamics*. Cambridge University Press.

TING, L. & TUNG, C. 1965 Motion and decay of a vortex in a nonuniform stream. *Phys. Fluids* **8**, 1039.

WIDNALL, S. E. 1972 The stability of a helical vortex filament. *J. Fluid Mech.* **54**, 641–663.

WIDNALL, S. E., BLISS, D. & TSAI, C.-Y. 1974 The instability of short waves on a vortex ring. *J. Fluid Mech.* **66**, 35–47.

WIDNALL, S. E., BLISS, D. B. & ZALAY, Y. 1971 Theoretical and experimental study of the stability of a vortex pair. In *Aircraft Wake Turbulence and Its Detection* (ed. J. H. Olsen, A. Goldburg & M. Rogers), pp. 305–338. Springer.

WIDNALL, S. E. & TSAI, C.-Y. 1977 The instability of the thin vortex ring of constant vorticity. *Phil. Trans. R. Soc. Lond.* A **287**, 273–305.